NON-DISSIPATIVE DECAY OF LINEAR QUASIMODES IN A PURE ELECTRON PLASMA

Thesis by

N. Sateesh Pillai

In Partial Fulfillment of the Requirements

for the Degree of

Doctor of Philosophy

California Institute of Technology

Pasadena, California

1995

(Submitted April 12, 1995)

ACKNOWLEDGMENTS

Research cannot be accomplished without a teacher from whom the student learns. I found this in Prof. Roy Gould and wish to thank him for his approach and patience. It's not easy for an electrical engineer to switch over to plasma physics. But Prof. Gould helped make that transition less troublesome and very rewarding in terms of experience and knowledge. I still have a lot to learn from his methodology, but time prevents me from continuing further.

My lab apprenticeship was carried out under the guidance of Dr. Michael LaPointe who offered advice as a teacher, friend and fellow human in the struggle for existence. His jovial manner and keen wit made research work very pleasant.

Professor Corngold provided an extremely useful source of dialog in mathematical physics and the philosophy of learning. I thank him for introducing me to the concept of quasimodes and for the useful advice that he renders every now and then.

Special thanks to Prof. Hardy Martel who made it possible for me to do research work in physics.

I wish to thank other faculty at Caltech and the institute in general. This includes my teachers in the various courses and the staff with whom I have interacted. Caltech is the only school I have studied where learning was a pleasure in the classroom, the laboratory as well as in the various activities in which I have been involved. Members of the Caltech community to whom I am grateful for their advice, encouragement and support include Frank Cosso, Reynold Johnson, Janice Tucker, Paula Samazan and Parandeh Kia. The group secretaries, past and present, deserve special mention for helping out with administrative and personal matters. They are Rosalie Rowe, Laura Rodriguez and Connie Rodriguez.

The Applied Physics coffee club, formerly administered by Laura Rodriguez and presently handled by Jana Mercado, helped alleviate the tedium of research by providing stimulating discussion and shots of caffeine. Thanks to both administrators.

My gratitude goes to the contract monitor, Dr. Charles Roberson of the U.S. Office of Naval Research, whose keen foresight provided continued funding for the pure electron plasma program at Caltech and other places.

Professor V. Ramnarayanan of the Indian Institute of Science, Bangalore (India), was instrumental in encouraging me to study at Caltech. His unique courses offered me a glimpse of what learning was like in Caltech.

My wife, Madhavi, has been closely associated with my research ever since my candidacy examination. Communications with her provided the much sought after consolation in an otherwise unemotional environment. Her presence during the past six months provided me with encouragement, understanding and patience. I learned from her what I could not learn from Caltech. I thank her for holding the proverbial carrot on a stick.

ABSTRACT

This thesis describes the first experimental observations of linear collisionless damping of perturbations in a pure electron plasma and provides the theoretical proof for collisionless damping in two dimensional inviscid incompressible fluids. Observations in the non-linear regime provide evidence for fluid trapping in the potential well of the perturbation.

The perturbations are in the form of diocotron waves which possess azimuthal symmetries described by the eigen number $m = 2$. The plasma is a cylindrical column of electrons confined in a Penning trap. Diocotron waves are excited by applying azimuthally propagating electric fields to the electrode structures forming the wall of the Penning trap.

Experiment shows that the damping of diocotron waves is not caused by dissipation at the electrode wall, and that the presence of such a dissipation decreases the decay rate of these waves, confirming that the $m = 2$ diocotron wave is a negative energy wave.

A self consistent set of equations for the perturbed potential is derived using the cold two dimensional fluid model. This results in the diocotron equation, which is the cylindrical plasma analog of Rayleigh's equation for shear flow of an inviscid incompressible fluid between parallel sheets. The complex form of the diocotron equation is solved, with homogeneous boundary conditions, for a particularly simple radial density profile showing that the diocotron resonances are quasimodes of the 2-D fluid. The solution reveals a complex eigenvalue which is consistent with the observed collisionless exponential damping of the diocotron wave in the linear regime.

Solution of the diocotron equation with more complicated density profiles is carried out numerically using the Runge-Kutta method on a computer.

CONTENTS

4. Diocotron Theory

5. Computational Results

6. Conclusion and Future Work

CHAPTER 1

INTRODUCTION

1.1 Historical Perspective

A plasma is a collection of charged particles that exhibit collective behavior. If a disturbance in the form of a test charge is introduced into the plasma, the influence of the disturbance would be attenuated by a factor of e at a distance equal to what is known as the Debye length. If the Debye length is less than the dimensions of the collection of particles, then the ensemble constitutes a plasma.

Plasmas are used in day to day life in the form of neon lamps and are the core material used for fusion, which may someday provide a clean source of power. They exist naturally throughout the universe in stars and also surround the earth in the form of the ionosphere. However, these naturally occurring plasmas are all neutral in the sense that there are equal number of oppositely charged particles. It is possible to have a *non-neutral* plasma, in which case overall charge neutrality is not maintained. It has been shown that non-neutral plasmas also exhibit Debye shielding and collective behavior [1]. Non-neutral plasma may be a collection of electrons or positrons or ions. The work described here was performed on a collection of electrons alone, a pure electron plasma.

Although the experimental study of pure electron plasma started only two decades ago, work on electron beams had been going on since the second world war. In the course of the investigations carried out on beams, it was found that hollow electron beams were unstable resulting in spontaneous vortex formation across the cross section of the beam [2, 3]. Analyses were carried out which showed that this instability was due to the shear of electron velocity transverse to the axis of the beam, and hence was termed as a "slipping stream" instability [4 – 7]. French scientists unsuccessfully attempted to utilize the instability to amplify electrical signals and created the "diocotron" tube [8]. The word is

derived from the Greek word "$\Delta\iota\omega\kappa\omega$" (dioco) for "I chase" which describes the shear nature of the electron velocity resulting in the instability. Although the tube did not survive, the name has, so that diocotron instability is more popular in usage than the term "slipping stream instability."

As the study of electron beams and diocotron instabilities was progressing, Levy in 1965 showed that a perfect analogy existed between electron dynamics in beams (under certain approximations) and the flow of an inviscid incompressible fluid [9]. This gave the beam physicist access to the body of literature on fluid dynamics which dealt with similar problems, dating all the way back to Rayleigh's landmark paper in 1880 where he derived the eponymous differential equation describing plane parallel flow [10]. Fluid work in this area included a prediction of vortex formation (Kelvin's cat's eyes) and asymptotic algebraic decay of streamline perturbations [11, 12]. Levy had shown that the diocotron instability could be derived from the two-dimensional (2-D) fluid model of the electron beam, with the unstable nature of the beam revealing itself in a singularity in the Rayleigh equation. The first substantial theoretical work on diocotron waves came out in 1970, when it was shown that cylindrical beams (or fluids) with a monotonically decreasing radial density (vorticity) profiles can have, at the most, only one neutral mode and no other eigenvalue [13].

Experimental work on confined pure electron plasma did not appear until 1975 [14]. Further study showed that it was possible to purposely excite diocotron waves of different azimuthal eigen numbers in such a plasma system, and that these waves are subject to parametric instability [15, 16]. The advantage of a plasma system in studying 2-D fluid dynamics was recognized and papers have been published dealing with vortex dynamics in a pure electron plasma [17 – 19].

A recent experiment on diocotron waves in a pure electron plasma with a monotonically decreasing density profile showed that these waves are damped in the linear regime [20]. The damping rate is fast enough that collisions could not account for it,

indicating a collisionless decay similar to Landau damping of plasma oscillations [21]. This is particularly intriguing in light of the fact that there are no complex eigenvalues for the model equation under these circumstances. More recent theoretical work shows that these waves are "quasimodes" of the plasma (fluid) system [22].

1.2. Thesis Outline

The work presented in this thesis is based on the experiment revealing linear collisionless decay of diocotron waves. This wave is shown to be a damped resonance of a pure electron plasma (two-dimensional inviscid incompressible fluid) with monotonically decreasing density (vorticity) profiles. Specifically, it is a characterization of an $m = 2$ diocotron wave. The letter m represents the azimuthal eigen number and signifies the existence of m vortex patches in the (r, θ) plane of a cylindrical column of electrons. The study is carried out by observing the currents induced on the walls of the electrode structure confining the plasma.

Chapter 2 provides a description of the experimental apparatus and associated instrumentation which enabled measurements in the linear regime to be carried out.

Chapter 3 describes the experimental observations made after exciting the plasma with a burst of sinusoidal signal. This burst introduces an azimuthally propagating electric field which travels at the same speed as a diocotron wave, thus exciting it. The same chapter also describes an experiment which shows that the diocotron waves are *negative* energy waves. That is, the presence of dissipation at the wall of the confining electrodes causes the wave damping rate to *decrease*, rather than increase. For sufficiently high resistances, damped $m = 2$ diocotron waves can be made unstable.

In Chapter 4, a theoretical study is carried out on the perturbations in the (r, θ) plane to derive the governing linear differential equation. The model so formed represents the differential equation for the streamline function in a two-dimensional inviscid incompressible fluid. The equation is solved for a particularly simple density (vorticity)

profile, to reveal that the diocotron waves are eigenvalues of the *complex* form of the differential equation.

The theoretical work is extended to more complicated profiles in Chapter 5, the extension being carried out by a numerical differential equation solver executed by a computer.

This thesis does not cover all the aspects of diocotron waves. Some assumptions are made in order to derive the model equation. And some experimental observations open up more questions. These points are discussed in Chapter 6.

REFERENCES

[1] R.C. Davidson, J. Plasma Phys. **6**, 229 (1971)

[2] O. Buneman, J. Electron. Control **3**, 1 (1957)

[3] H.F. Webster, J. Appl. Phys. **26**, 1386 (1955)

[4] O. Buneman, J. Electron. Control **3**, 507 (1957)

[5] R.L. Kyhl and H.F. Webster, IRE Trans. Electron Dev. **3**, 172 (1956)

[6] J.R. Pierce, IRE Trans. Electron Dev. **3**, 183 (1956)

[7] G.G. McFarlane and H.G. Hay, Proc. Phys. Soc. **63**, 409 (1953)

[8] A.H.W. Beck, Space Charge Waves and Slow Electromagnetic Waves (Pergamon Press, 1958)

[9] R.H. Levy, Phys. Fluids **8**, 1288 (1965)

[10] J.W.S. Rayleigh, Proc. London Math. Soc. **11**, 57 (1880)

[11] W. Thompson, Nature **23**, 45 (1880)

[12] K.M. Case, Phys. Fluids **3**, 143 (1960)

[13] R.J. Briggs, J.D. Daugherty and R.H. Levy, Phys. Fluids **13**, 421 (1970)

[14] J.H. Malmberg and J.S. deGrassie, Phys. Rev. Lett. **35**, 577 (1975)

[15] J.S. deGrassie and J.H. Malmberg, Phys. Fluids **23**, 63 (1980)

[16] T.B. Mitchell, C.F. Driscoll and K.S. Fine, Phys. Rev. Lett. **71**, 1371 (1993)

[17] C.F. Driscoll and K.S. Fine, Phys. Fluids B **2**, 1359 (1990)

[18] K.S. Fine, C.F. Driscoll, J.H. Malmberg and T.B. Mitchell, Phys. Rev. Lett. **67**, 588 (1991)

[19] A.J. Peurrung and J. Fajans, Phys. Fluids A **5**, 493 (1993)

[20] N.S. Pillai and R.W. Gould, Phys. Rev. Lett. **73**, 2849 (1994)

[21] L. Landau, J. Phys. (Moscow) **10**, 25 (1946)

[22] N.R. Corngold, Phys. Plasmas **2**, 620 (1995)

CHAPTER 2

EXPERIMENTAL OUTLINE

2.1 INTRODUCTION

In order to work with a pure electron plasma, it must be possible to produce electrons and confine them to a plasma while experiments are conducted. A very easy way of producing electrons is by heating a biased thoriated tungsten filament kept in vacuum. Once the electrons are emitted, it is a simple matter of collecting them together into a confinement chamber. A commonly used confinement chamber is the cylindrical Penning trap shown in Figure 1 where the electrons are trapped within a segmented cylindrical electrode structure. Trapping cannot be achieved without a steady-state magnetic field. This will curb the mutual electrostatic repulsion between particles and cause them to be in steady-state rotation. Theoretically, such a plasma should be confined forever. In practice, some particles are lost due to anomalous transport processes [1]. The time by which the total number of electrons decays to some fraction (say half) of its initial value is considered as the confinement time. It has been shown empirically that confinement time scales as the square of the confining magnetic field and is independent of the background neutral pressure when the pressure is below 10^{-6} Torr [1]. The experiments described in this thesis are performed at pressures around $5x10^{-8}$ Torr with a steady-state magnetic field of 50G. This gives a confinement time of the order of about 100ms. Experiments on such plasma must be completed before loss of particles causes the density to degrade considerably. The particles that remain within the confinement region at the end of the experiment are dumped onto a collector. Since the hot filament still evaporates electrons, another plasma can be made and experimented upon after the previous plasma

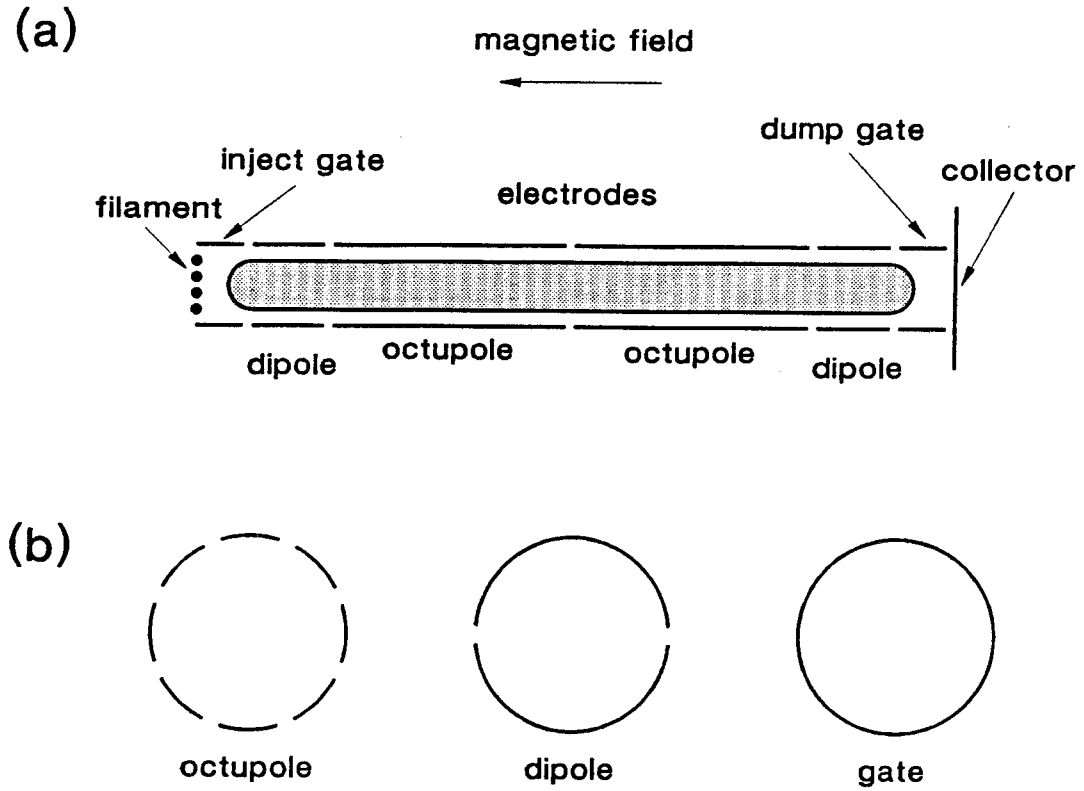

Figure 1(a) Schematic of Penning trap used to confine the pure electron plasma. Entire structure is kept under vacuum pressure of about 5×10^{-8} Torr. An axial magnetic field is used to radially confine the electrons, while negative electrostatic potentials applied to the inject gate and dump gate electrodes allow axial confinement. In the region where the electrons are trapped, the electrodes are axially segmented to allow different multipole electric fields to be excited within the plasma. (b) End-view of different electrodes showing azimuthal sectoring. Electrical signals of different phases may be applied to different sectors of the octupoles and dipoles.

has been dumped. In this manner, electrons are generated, confined, experimented upon, and finally dumped onto a collector. This is a common repetitive cycle used to perform experiments on non-neutral plasma. Since a single confinement will last only around 200ms, many repetitions of the confine-experiment-dump cycle may be performed in quick succession.

The experiments that are performed on the plasma must take place within the 200ms duration of trapping. CAMAC (Computer Automated Measurement And Control) modules are used to automate the process of excitation and recording the plasma response. In this way, the plasma response may be recorded on a repetitive basis allowing data to be recorded in a short time.

The response of the plasma is in the form of a decaying sinusoid (see Figure 10). Typically, 20 sets of plasma responses are digitized for a single set of experimental settings. The 20 digitized responses are used to average out the random variations between responses. The signal that is averaged is not the actual response (Figure 10), but the envelope of the response (Figure 11). Random variations between plasma responses include random glitches and variations in the electron emission from the filament. Both of these changes result in a slight alteration of the steady state density profile. The plasma response is digitized as fast as possible before significant long-term of the density profile occur.

2.2 VACUUM SYSTEM

The basic structural setup of the experiment is shown in Figure 2. The electrode structure confining the plasma is kept inside the horizontal section of the vacuum chamber which fits through the axis of fourteen discrete coils producing the steady-state magnetic field. The vacuum pressure of $5x10^{-8}$ Torr is maintained by an NT450 turbo molecular

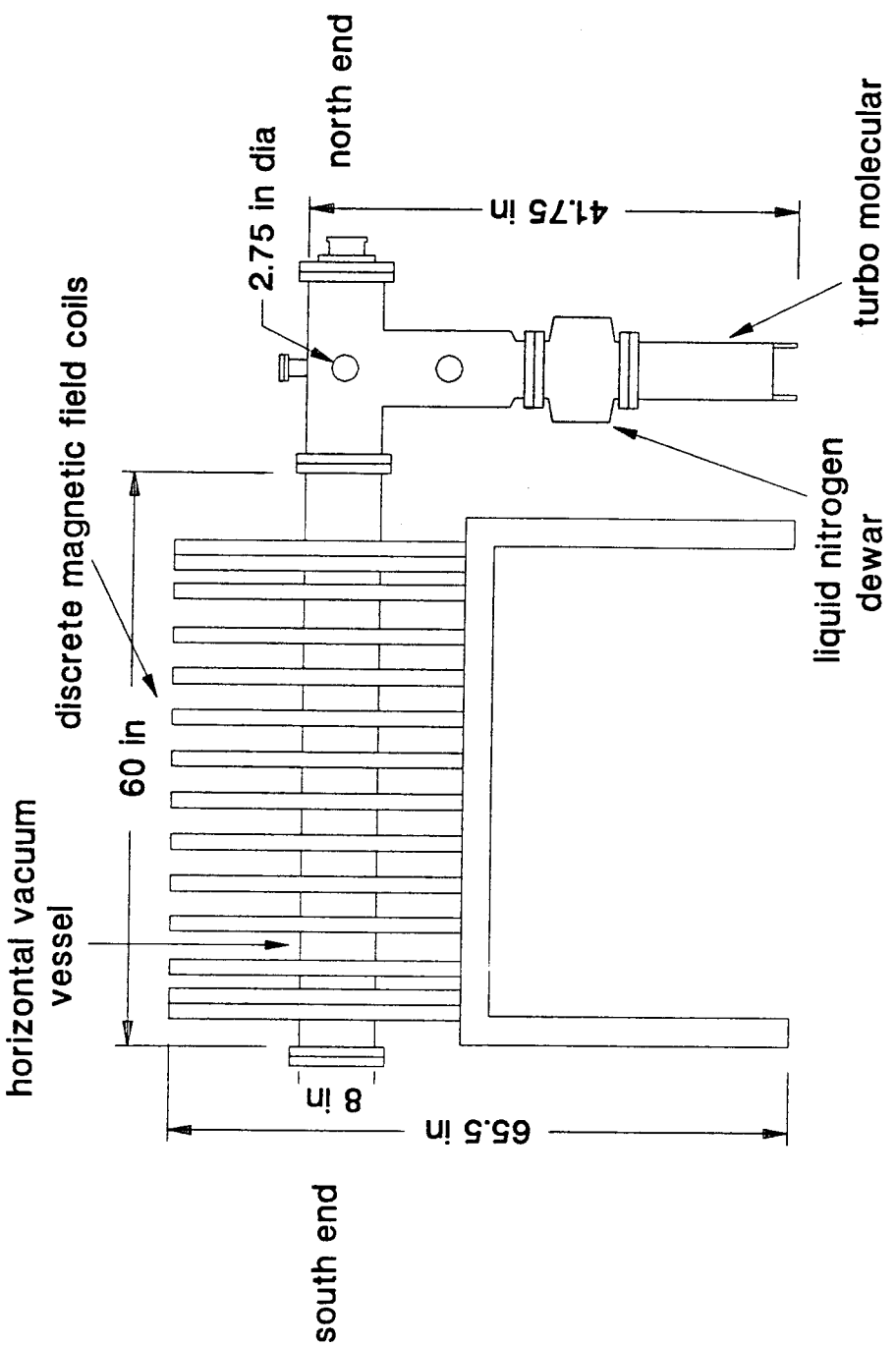

Figure 2. Diagram shows setup of the vacuum chamber and magnetic field coils. Electrode structure, where experiments on the plasma are carried out, rests in the middle of the horizontal vacuum vessel. Compensation coils producing horizontal and vertical magnetic fields are wound on a frame placed outside the horizontal vessel and through the axis of the main field coils.

pump followed by a mechanical roughing pump. A liquid nitrogen cold trap interfaces the turbo pump with the vacuum chamber. This helps to reduce the turbo pump lubricating oil that may back-stream into the vacuum chamber. Measurements of the vacuum are made by a nude ion gauge connected to a Varian ratiomatic ion gauge controller.

Calculations show that for 2eV electrons with a density of $10^6 cm^{-3}$ and a background neutral pressure of $5x10^{-8}$Torr, the mean time between electron-electron collisions is around 50ms and the mean time between electron-neutral collisions is around 20ms (assuming the background neutral is pure nitrogen).

2.3 MAGNETIC FIELD

The 14 discrete coils were chosen to produce the magnetic field for the simple reason that they were already in the lab. Hence it was decided not to wind a solenoid. These coils are flat "pancakes" about 36"x32"x1$\frac{3}{4}$" with a 12" diameter bore. The internal wires are wound around the axis of the bore, providing an axial magnetic field without any poloidal component. The coils are aligned and the vacuum chamber positioned along the axis of the coils, supported by X supports at the two ends. Coils are numbered starting with #1 at near the vacuum pump and #14 at the end flange. Inter-coil spacings were carefully calculated to produce a uniform magnetic field in the middle of the vacuum chamber where the electrode structure would rest. The spacings so calculated are shown in Table 1. Other factors also influence the magnetic field, such as the stray ambient field and slight coil dissimilarities. As a result, the field is not as uniform as calculated. In order to compensate for these influences, variable trimming resistors were placed across each coil to shunt small amounts of current from the individual coils. The value of the effective resistance used to shunt current so as to produce a uniform field at 50G are shown in Table 2. The resulting magnetic field (at 20G) is shown in Figure 3 and is uniform to

between coils	spacing (in)
1 and 2	0
2 and 3	1.375
3 and 4	2.963
4 and 5	2.616
5 and 6	2.704
6 and 7	2.708
7 and 8	2.725
8 and 9	2.708
9 and 10	2.704
10 and 11	2.616
11 and 12	2.963
12 and 13	1.375
13 and 14	0

Table 1. Spacing in inches between various coils. This spacing is done so as to get the maximum uniformity within the region where the electrode structure rests (and hence where the plasma is confined).

coil #	effective shunt resistance (Ω)
1	122.7
2	53.68
3	19.23
4	9.08
5	9.48
6	10.2
7	8.68
8	8.88
9	11.13
10	16.83
11	14.2
12	14.08
13	9.53
14	10.73

Table 2. Effective shunt resistance used for each coil to compensate for ambient field and differences between coils. Actual resistors used were 1% tolerance resistors in parallel with a series combination of a 100Ω potentiometer and a 27Ω resistor.

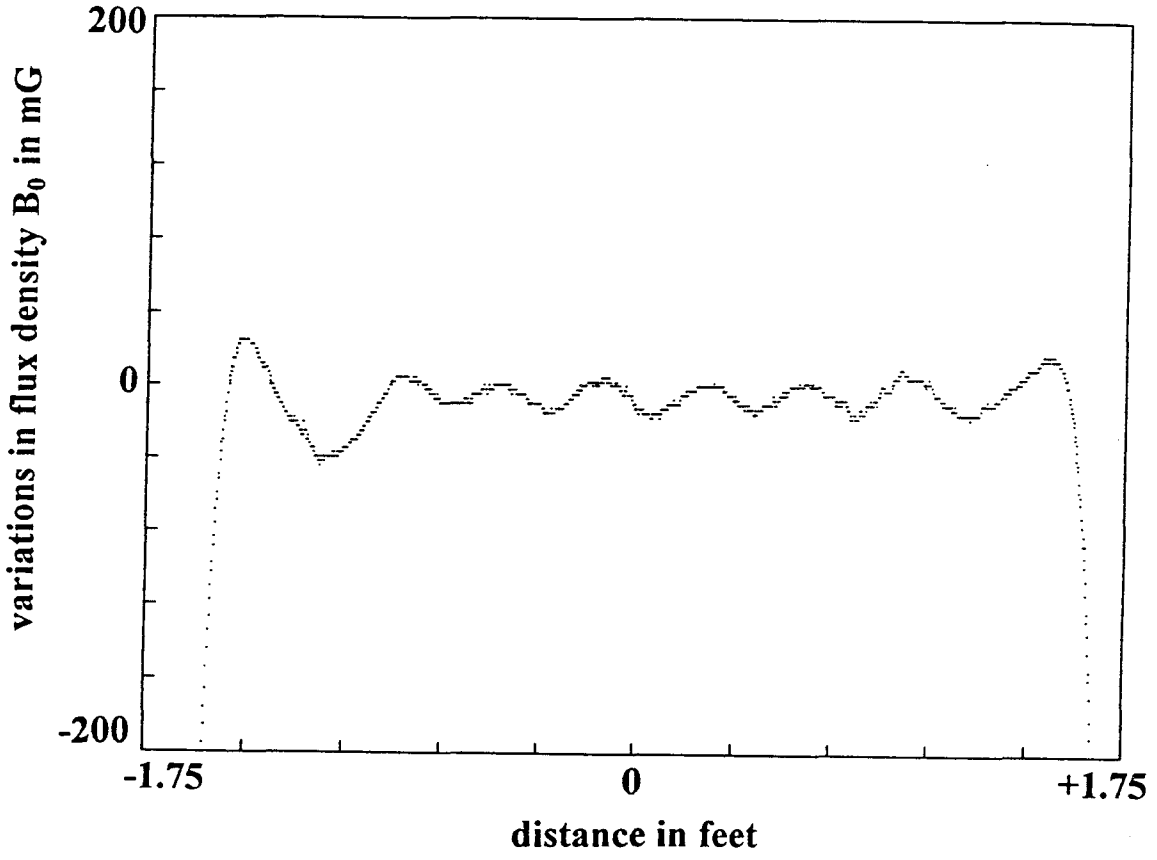

Figure 3. Variations in the axial field B_0 as a function of the distance from the center of the magnetic coils. The zero on the vertical axis corresponds to an actual flux density of about 20G. The zero on the horizontal scale corresponds to the midpoint between coil 1 and coil 14. Ripples in the field are caused by the discrete coils, the valleys corresponding to the spaces between the coils. Measurement was taken for a 20G field produced by a current of 2.4A as measured by a hall effect probe connected to a Bartington model MAG-01 fluxgate magnetometer.

within 0.03% and directed the same way as the horizontal component of the terrestrial field.

In addition to the main confining magnetic field, there are two compensating coils to alter the vertical and horizontal fields. The currents in these coils would be set during experiment and adjusted to achieve optimum experimental performance. Most often they are used to obtain maximum confinement time, which may vary from day to day. Typical values of current used are, say, 200mA for either coil.

2.4 ELECTRODE STRUCTURE

The electrode structure used in confining the plasma consists of gold plated copper segments connected together to form a cylinder with azimuthally sectored electrodes as seen in Figure 1. Different segments have different purposes. The filament is attached to a cylindrically symmetric segment which forms the north end of the structure. An anode grid is attached to the other end of this segment. Other electrodes appearing in order to the south end are: a cylindrical "inject" gate, a dipole with two azimuthal sectors, an octupole with 8 sectors, another octupole with 8 sectors, a second dipole with 2 sectors, a cylindrical "dump" gate, and a collector. Each segment of electrodes is separated from the other by means of hollow grounded disk plates which help to suppress noise between electrodes. When the plasma is normally trapped, the inject and dump gates are held at $-100\,\mathrm{V}$, preventing any electrons from escaping in the axial direction. At the end of experimenting, the dump gate potential is increased to around $+1.5\,\mathrm{V}$ and kept at that voltage for $25\,\mu\mathrm{s}$, allowing the electrons to be dumped to the collector plate to which a nominal $+10\,\mathrm{V}$ is applied. At the end of $25\,\mu\mathrm{s}$, the dump gate voltage is returned to $-100\mathrm{V}$. When the next batch of electrons are to be confined, electrons from the filament are allowed to move into the "trap" region (consisting of the region under the dipoles and octupoles where the experiments are carried out) by gating the inject gate to $+1.5\,\mathrm{V}$ for

25 μs. The trap cannot be overfilled. Electrons from the filament will move into the trap only as long as the electrostatic potential in the trap is higher than the filament potential. At the end of 25 μs, when the inject gate voltage is changed back to -100 V, the electrons in the trap region would have a radial potential distribution similar to that of the filament. For this purpose, the filament has a bias of -30 V applied to it at all times. The filament bias is applied to the center of the filament. The current through the filament will cause a potential drop in the filament increasing from -30 V at the center to around -20 V at the outer spiral. Thus electrons from the filament are emitted, trapped and dumped.

All the electrodes are electrically connected to SMA coaxial connectors on the south end flange of the vacuum vessel. Each sector of an octupole or dipole has an independent terminal so that different voltages may be applied to different sectors of the same electrode segment. Connections to any electrode are made from instruments located in a small control room to the flange terminals by means of RG-58 coaxial cables. The filament and the magnetic field terminals have separate high current cables. Normally the filament is run with a current of 8A while the confining magnetic field coils require 6A to produce 50G.

The magnetic field on the axis of the filament, in the plane of the spiral, due to the filament current is about 33G. If this filament field were opposite in direction to the confining field of 50G, a cusp field would be produced diverting the electrons emitted from the filament away from the trap region. Hence, care was taken during the assembly to see that the filament field was in the same direction as the confining field. Another requirement is that the outer spiral of the filament be at a higher potential than the inner spiral, so as to match the potential of the plasma as it is being trapped. This means the current in the filament must be in a direction so that the outer spiral has a potential higher than the inner spiral. This is ensured by winding the spiral with the proper orientation.

A summary of the parameters of the resulting plasma is shown in Table 3.

EXPERIMENTAL PARAMETERS

magnetic field	50 G
central electron density	$\approx 1 \times 10^6 \mathrm{cm}^{-3}$
plasma temperature	2 eV
cylinder radius	2.5 cm
trap length	40 cm
trap duration	200 m (typical)
trap repetition rate	5 Hz (typical)
cyclotron frequency	140 MHz
central plasma frequency	$\approx$ 9 MHz
wall rotation frequency	150 kHz (typical)
$m = 2$ diocotron frequency	500 kHz (typical)
axial bounce frequency	1 MHz
Larmor radius	1 mm
Debye length	1 cm

Table 3. Parameters of the pure electron plasma. The central electron density and central plasma frequency are calculated by assuming that the normalized density profile, $f(\rho)$, varies with normalized radius, ρ, as $f(\rho) = (1 - \rho^2)^3$, with the plasma edge at 80 % of the cylinder radius. Plasma temperature is measured using the technique described in reference 2.

2.5 EXPERIMENTAL PROCEDURE

Once the electrode structure is in vacuum at a pressure of $5x10^{-8}$ Torr after baking, the setup is ready to run pure electron plasma experiments. Connections are made to ensure proper inject-experiment-dump sequence for the plasma. This involves setting up the magnetic field to 50G, running a filament current of 8A, and setting up the proper timing sequence for injecting, trapping and dumping the electrons. The timing sequence is generated through the CAMAC crate through software from a 386 based IBM compatible computer. Electrons that are dumped onto the collector are passed through a unity gain charge amplifier to detect how much charge has been collected. This provides the most useful diagnostic that electrons have indeed been trapped and dumped. The dumped charge is in fact a function of the time for which the plasma has been confined, electrons being lost by virtue of anomalous transport. A record of the variation of dumped charge vs. duration of confinement (in ms) is obtained by digitizing the dumped charge for different confinement periods (trap duration) in ms. Such a plot, known as a confinement plot, is a very useful diagnostic in obtaining information about filament emission as well as confinement time. A typical confinement plot is shown in Figure 4. Another useful diagnostic is the record of the emission current. Typical emission currents on a "good day" are between 100μA and 160μA for a filament bias of -30 V, filament current of 8A and an axial field of 50G.

Once a steady inject-trap-dump cycle has been established, and the confinement time and emission current are "good" the plasma is ready for experiments. In order to excite an $m = 2$ diocotron resonance in the plasma, a 5μs burst of sine wave is applied to one octupole segment with an $m = 2$ symmetry. The typical frequency for this sine wave is 500kHz, and is obtained from a Wavetek model 166 signal generator. The setup is shown in Figure 5. One sector of the other octupole segment is used to detect the response of the plasma and is therefore connected to a low-noise amplifier. All other

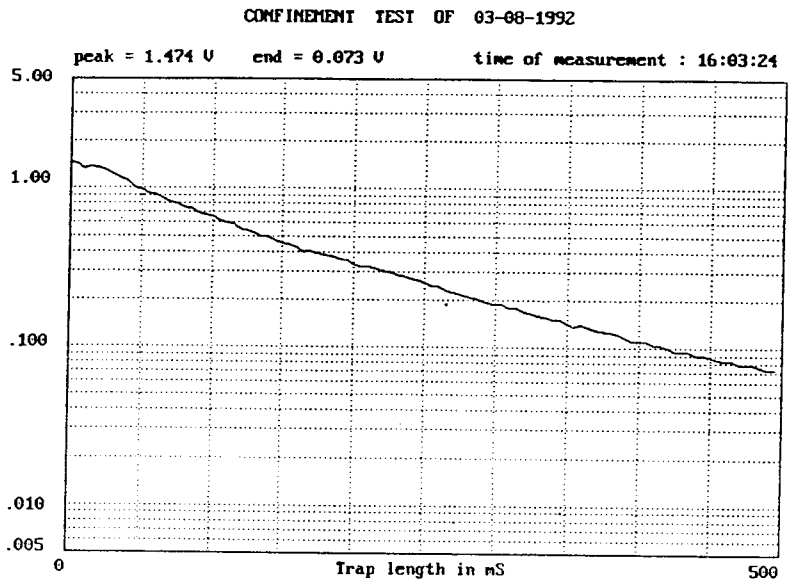

Figure 4. A typical confinement plot showing the total dumped charge developed over the line capacitance vs. duration of confinement plotted on a semilog graph. The charge developed over the line capacitance (about 150pF) is measured directly in volts. The numbers on the y-axis correspond to these voltages. Numbers on the top line indicate peak voltage (for minimum confinement duration) and the voltage for the longest confinement duration. The time required for the total charge to decay by half in this particular case is around 100ms.

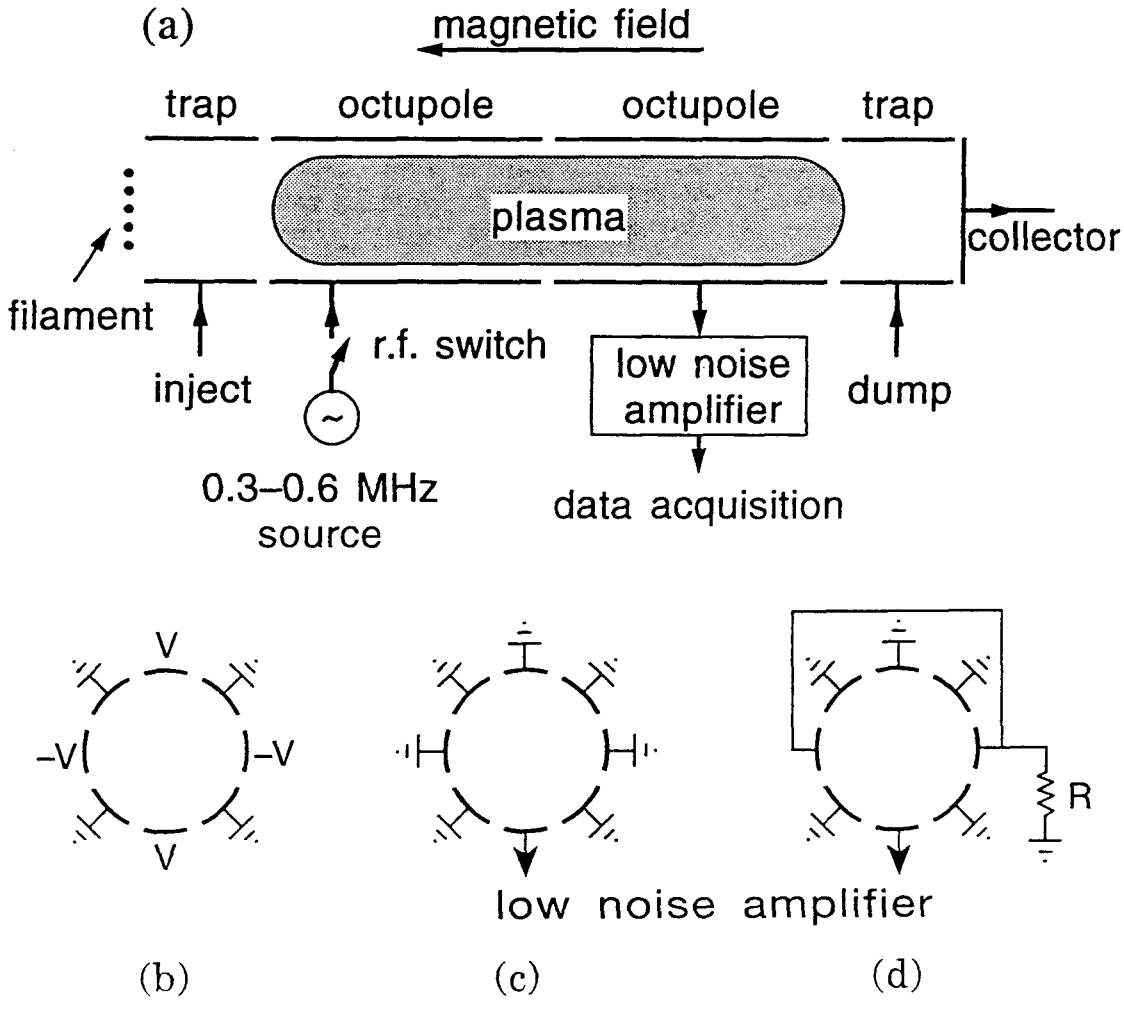

Figure 5. (a) Schematic of cylindrical structure for plasma trapping and excitation, (b) phasing of first octupole for exciting an m=2 disturbance, (c) configuration of second octupole for signal reception, and (d) configuration of second octupole for negative energy test.

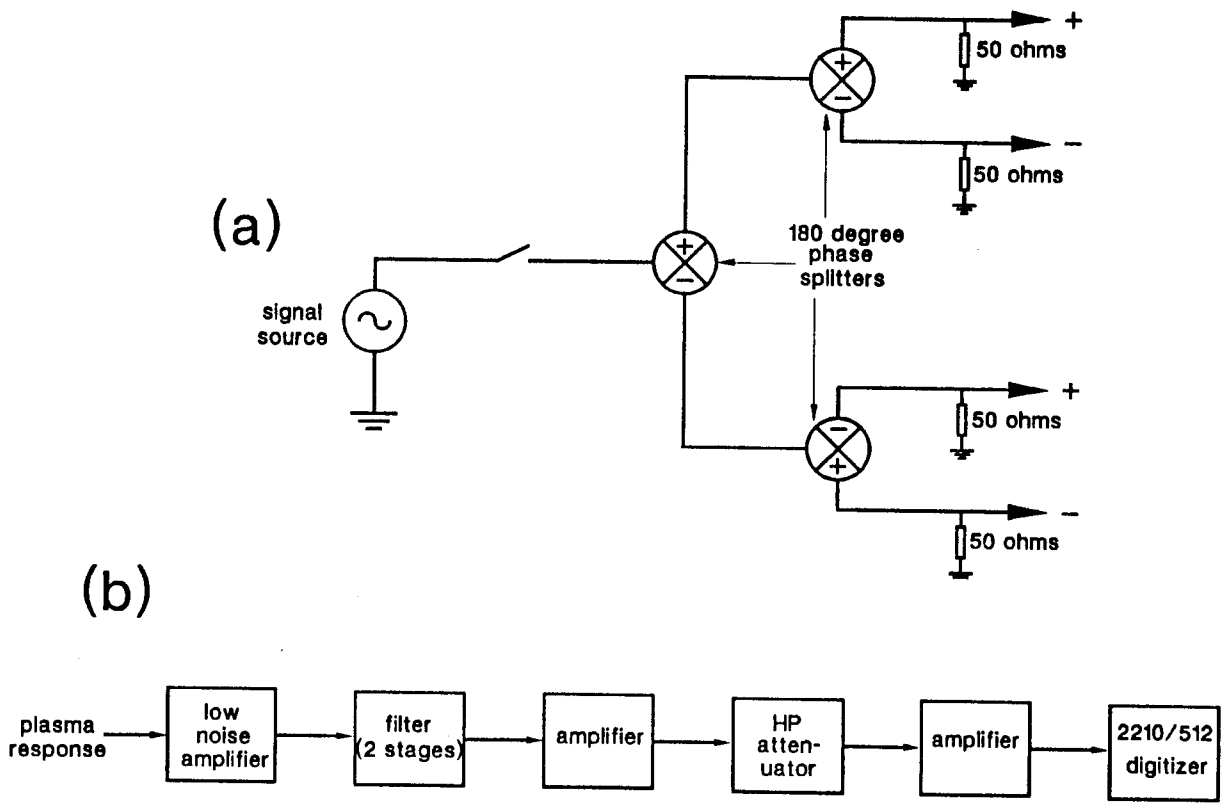

Figure 6. (a) Setup for generating the signals to excite the plasma. Signal from a generator is passed through two stages of phase splitting to obtain the proper phases to be applied to the octupole sectors. (b) Block diagram shows the various stages of processing of the received signal (plasma response) before digitization. The plasma response is an induced current in the wall of the octupole sector.

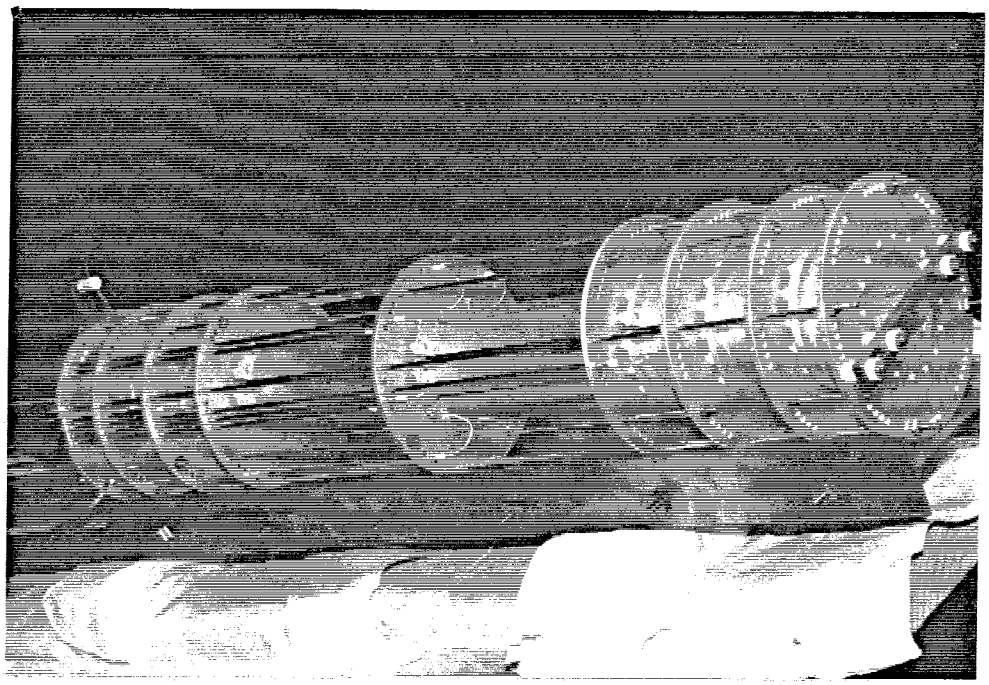

Figure 7. The electrode structure where the electrons are generated and trapped. Circular rings separate the various electrodes which are made of gold plated copper. The right end of the photograph shows the electrode to which the filament is attached.

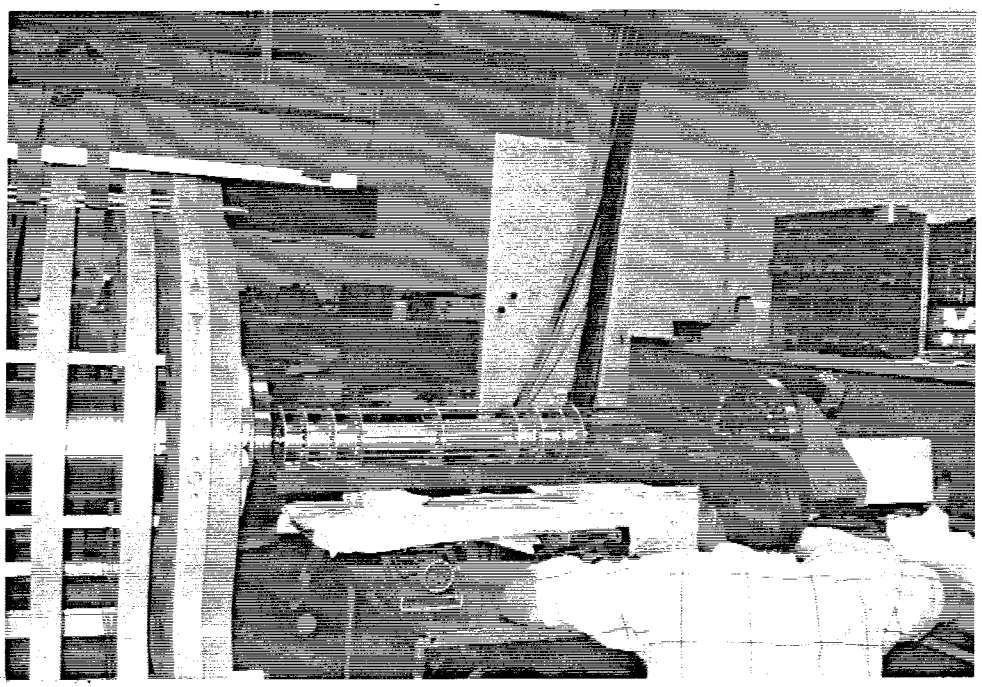

Figure 8. The Penning trap with all the electrodes connected to the end flange by means of rigid coaxial cables. The structure is just about to enter the vacuum chamber from the south end of the vacuum chamber.

sectors of the octupoles and dipoles are at d.c. ground. The low noise amplifier consists of an Amptek A250 hybrid amplifier at the front end, followed by two stages of non-inverting and buffer amplifiers. This configuration gives a measured mid-frequency gain of 22,500 with a 3-dB bandwidth from 2.2kHz to 1.5MHz and a noise density, measured with a 50Ω input resistance, of 5.3 $nV/\sqrt{Hz}$. A block diagram representing the processing of the applied and received signals are shown in Figure 6. The received signal, after being amplified by the low-noise amplifier located directly at the flange, is passed through two filter stages, an HP attenuator and another amplifier before being digitized by a DSP model 2210/512 transient recorder. Overall amplification is of the order of 2,000,000, so that the smallest signal level at the input to the digitizer is about $\pm$ 1V.

REFERENCES

[1] J.H. Malmberg and C.F. Driscoll, Phys. Rev. Lett. **44**, 654 (1980)

[2] R. W. Gould and M. A. LaPointe, Phys. Fluids B **4**, 2038 (1992)

CHAPTER 3

EXPERIMENTAL RESULTS

3.1 INTRODUCTION

As discussed in the previous chapter, experiments are performed on the plasma after electrons are injected into a trap region within the Penning trap. When the electrons are trapped, they will form a cylindrical column of plasma. The particles will be distributed throughout the cylinder moving in the axial as well as azimuthal directions while radial motion is hindered by the confining magnetic field. Interaction between the strong electrostatic repulsion of similarly charged particles and the magnetic field produce a steady-state azimuthal motion of particles about the axis of the cylinder. Axial motion will consist of particles bouncing back and forth between the electrostatic traps at the two ends. For the purposes of understanding the experiment, the axial motion is neglected but is assumed to average the perturbations throughout the plasma column. The plasma thus consists of a column of fluid (using the 2-D fluid analogy) rotating about its axis.

The steady-state azimuthal fluid angular velocity, $\omega_0(r)$, depends on the steady-state density, $n_0(r)$, which is a function of the radius. Hence, different layers of the fluid rotate about the axis at different velocities. It is assumed that the density is highest on the axis and decreases monotonically towards the electrode wall. Figure 9 shows a possible radial density profile and the associated angular velocity.

3.2 THE IDEA OF A DIOCOTRON RESONANCE

It has been shown that the pure electron plasma has low frequency resonances located around the angular rotation frequency of the plasma [1, 2] . These are the diocotron resonances whose frequencies are low in comparison with the cyclotron frequency (around 140MHz for a 50G magnetic field). They occur when an azimuthally

propagating perturbation has the same phase velocity as the speed of angular rotation at a particular radius (the "resonant radius"). These propagating disturbances are assumed to vary as $e^{im\theta - i\omega t}$ and are distinguished by an azimuthal eigen number m, indicating the number of symmetric vortex patches that propagate in the azimuthal direction. This gives the perturbation a frequency ω and a wave speed ω/m. For some density profiles (which are not monotonically decreasing), the diocotron disturbance can arise spontaneously from noise resulting in diocotron instabilities, a disease that had plagued hollow beam electron tubes in the early days of beam tube devices [3 – 8]. A criterion to be satisfied for the occurrence of this instability in fluids flowing between parallel sheets was given by Rayleigh when he stated that the velocity profile must necessarily have a point of inflection. For a fluid of electrons in the cylindrical geometry, a monotonically decreasing density profile is a guarantee against spontaneous diocotron instabilities provided the cylinder wall is a perfect conductor. It is possible to forcibly excite a diocotron resonance by purposely inducing a traveling electric field within the plasma [1, 2]. This may be done by applying appropriate potentials to the electrodes. In order to excite the perturbations of a particular azimuthal eigen number m, the applied voltage should posses the same angular symmetry as the perturbation. This is done using the octupole sections and the setup shown in Figures 5(b) and 6(a). Resonance occurs when ω, the frequency of the applied voltage, equals $m\omega_0(r_s)$ for some radius r_s where $0 < r_s \leq b$, and b is the radius of the wall.

It has been shown, both experimentally and theoretically, that the $m = 1$ diocotron resonance is an undamped, or lightly damped, resonance with a frequency, ω, exactly equal to the rotation frequency $\omega_0(b)$ at the wall [1, 2, 9, 10]. Experimentally, deGrassie had shown that the $m = 2$ diocotron has a frequency roughly 3 times $\omega_0(b)$, but is highly damped in comparison with the $m = 1$. It was also shown that the decay rate of the $m = 2$ response always decreased with the applied voltage. He states explicitly in

reference 2 that he was unable to reach the *linear* regime of the plasma response because of a low signal to noise ratio with the receiver setup.

3.3 THE EXPERIMENT

The experiment consists in perturbing the plasma, that has density and angular velocity profiles similar to that shown in Figure 9, with a rotating electric field at the wall of one of the octupole segments possessing an $m = 2$ symmetry using the setup shown in Figure 6(a). This is done by applying voltages to the electrodes of the octupole segments using phases as shown in Figure 5(b). The applied voltage will set up a standing wave within the plasma consisting of two waves traveling in the opposite azimuthal directions, but the plasma responds to the wave traveling in the direction of plasma rotation. The field at the wall has the form $E\cos(m\theta)\cos(\omega t)$, where ω is the radian frequency of the applied sinusoid and E is the electric field. The applied field is not a continuous sine wave, but a 5μs burst containing a few complete cycles and therefore contains a broad band of frequencies centered around the frequency of the applied signal, which is typically 500kHz. This will induce perturbations in the plasma that will produce a perturbed electric field at the wall which induces perturbed currents into the electrode. The induced current is then detected by means of the receiver setup shown in Figure 6(b). A charge proportional to the induced current will be seen at the input of the low noise amplifier, which converts it into a voltage for further processing. Thus the perturbed electric field at the wall, which is a measure of the plasma response, is detected and digitized.

When an $m = 2$ pulse of some voltage is applied to the plasma, it is found that the amplitude of the plasma response is maximum only at one particular frequency, indicative of resonance. Moreover, the plasma response increases linearly with time for the duration of the applied pulse when the frequency of the signal generator is tuned to the frequency at which the plasma response is a maximum. This confirms the presence of a resonance. The

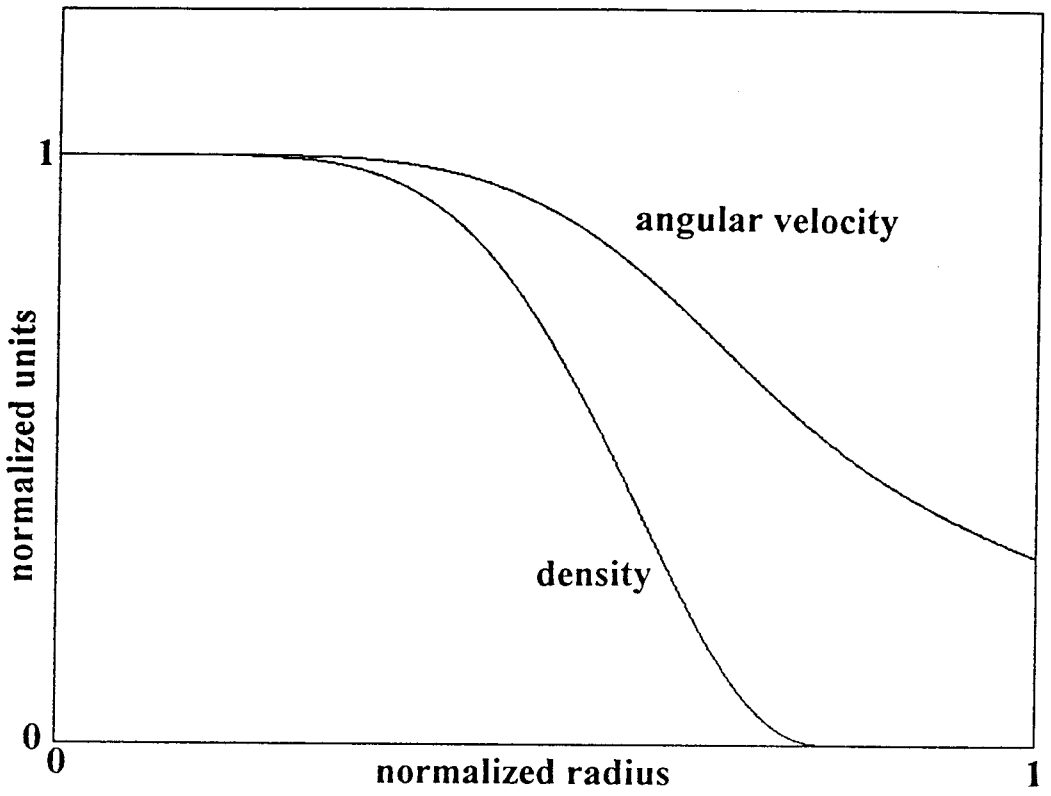

Figure 9. A plot of the radial variation of the normalized steady-state angular velocity $g(\rho) = 1 - \frac{5}{2}(\rho/\alpha)^6 + 3(\rho/\alpha)^8 - (\rho/\alpha)^{10}$ and normalized steady-state density $f(\rho) = 1 - 10(\rho/\alpha)^6 + 15(\rho/\alpha)^8 - 6(\rho/\alpha)^{10}$ where α is the ratio of the plasma edge radius to the cylinder wall radius, a/b, and ρ is the radius variable normalized to the wall radius. In this particular case, $\alpha = 0.8$. This density profile has the characteristic of being smooth at the plasma edge because $g(a) = \left.\frac{dg}{d\rho}\right|_{\rho=\alpha} = \left.\frac{d^2g}{d\rho^2}\right|_{\rho=\alpha} = 0$.

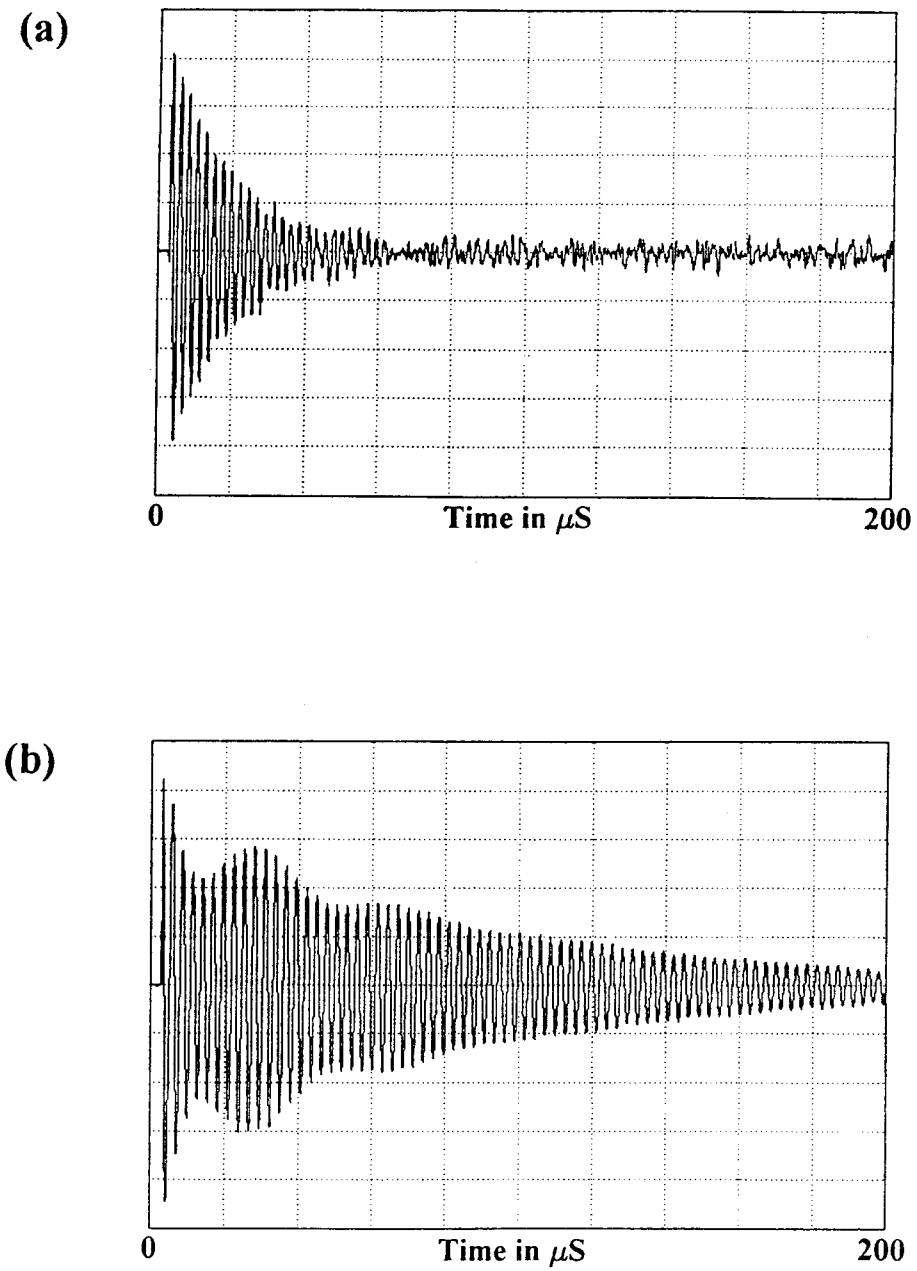

Figure 10 (a). A plot of the digitized plasma response to an $m = 2$ excitation for an applied voltage of 40mV. (b) The same plasma response, but for an applied voltage of 500mV. Main differences between (a) and (b) are (i) the decay rate is smaller for (b) and (ii) the plasma response in (b) seems to indicate a phenomenon resulting in amplitude modulation. The amplitude scales are different between the two figures, the response in (b) being attenuated by 19dB more than the one shown in (a).

frequency at which this resonance occurs is typically about 500kHz, between 2-4 times the $m = 1$ frequency, the lack of precision being caused by the non-reproducible nature of the plasma between successive trap cycles. As stated before, the plasma response rises linearly with time during the duration of the applied pulse. When the applied pulse is removed at the end of 5μs, the plasma response decays. A typical $m = 2$ response for low applied voltage is shown in Figure 10(a). Figure 10(b) shows the response for a higher applied voltage.

3.4 RESULTS

(a) LINEAR COLLISIONLESS DECAY

As can be seen in Figures 10(a) and 10(b), the plasma response for a low applied voltage is an exponentially damped sinusoid. As the applied voltage is increased, the exponential decay becomes *modulated* with a lower frequency sine wave and shows a decrease in the damping rate. It is possible to obtain the envelope of the response and plot the various response envelopes for different applied voltages on the same graph. Figure 11 shows such a plot where the envelope of the responses for a two decade variation of applied voltages is plotted on a semilog graph. Each trace on this graph represents the average of the envelopes of 15-20 responses for the same applied voltage. The bottom four traces are approximately linear on the semilog plot. For these four traces, the amplitude of the peak response (at $t = 0$) scales with the applied voltages of 10, 20, 40 and 60mV. These four traces represent the *linear* response of the plasma, by definition of linearity. Moreover, the time scales in which the decay occurs, 60μs, is much smaller than the mean time between collisions which is of the order of milliseconds. Hence the linear response of the plasma is that of an exponentially damped sinusoid, the damping being caused by a *collisionless decay* process. Measurements of the ratio of the frequency of the plasma response to the damping rate show that this ratio is 84 in the linear regime. The Q

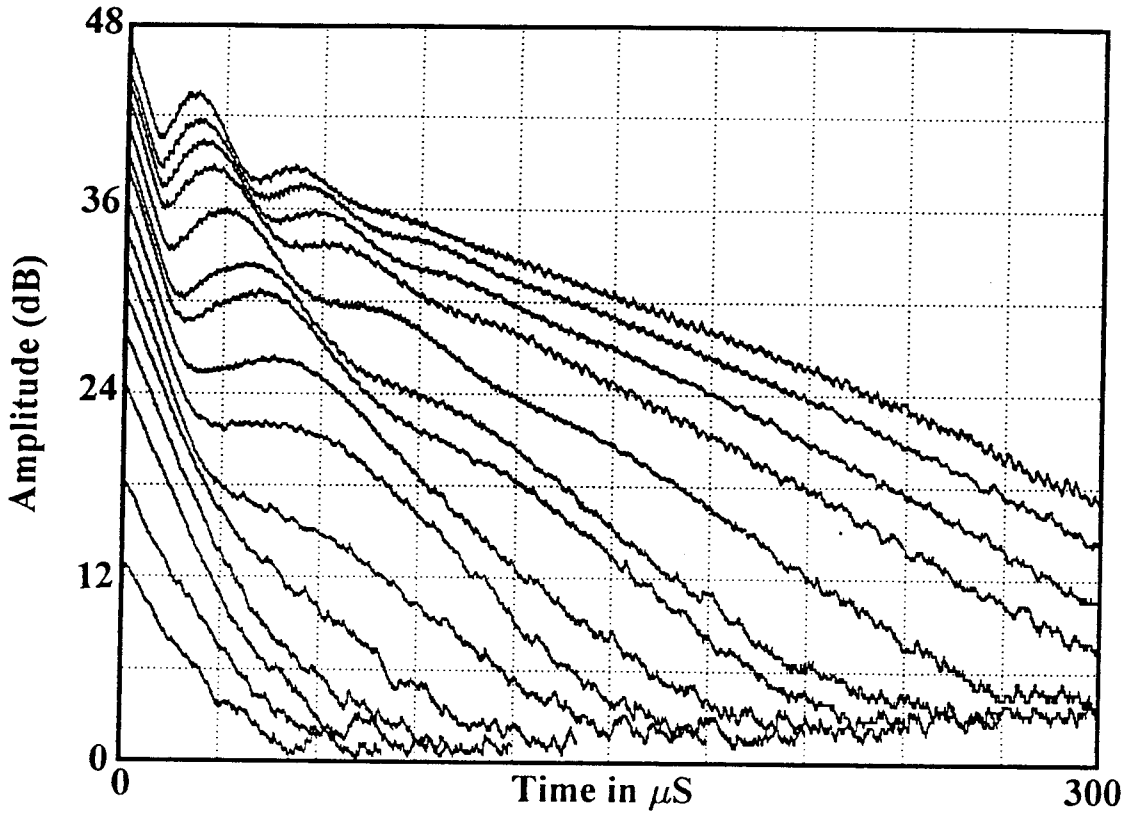

Figure 11. Decay of the envelope of the response to an $m = 2$ excitation. Responses are, in order from the bottom trace to the top trace, in response to applied voltages of 10, 20, 40, 60, 80, 120, 160, 200, 250, 300, 400, 500, 600, 700, 1000 mV. Plotted on a semilog scale with the vertical scale calibrated in dB.

of the diocotron resonance is half this value, or $Q = 42$. The theory behind the collisionless decay and a model for its occurrence is presented in detail in Chapter 4. As the amplitude of the applied voltage is increased, the plasma response shows signs of amplitude modulation by another signal whose frequency is much smaller than the frequency of the $m = 2$. It is clear from Figure 11 that signs of this amplitude modulation begin to appear in the trace showing the plasma response for an 80 mV applied voltage. However, it is more distinct for the larger applied voltages. Also apparent is that the frequency of the modulating signal *increases* with increasing applied voltage. It will be shown below that the frequency of the modulating signal is proportional to the square root of the applied voltage, providing evidence for fluid element *trapping* or *bouncing* within the potential well of the diocotron wave. Another noteworthy point in Figure 11 is that the decay rate of the plasma response to higher applied voltages *decreases* at later times, a phenomenon already studied by deGrassie in reference 2.

(b) FLUID TRAPPING

The evidence for fluid element trapping may be seen by plotting the modulating signal frequency against a *corrected* applied voltage. Care must be taken to obtain the modulating signal frequency from the data shown in Figure 11. For a single trace, say the response to 1000mV, it is seen that the modulating frequency decreases as the plasma response decays. The plasma response decays because the electric field at the wall decays, in response to the decay of potential within the plasma. Hence the potential at the radius, r_s, where the "trapping" or "bouncing" occurs also decays. This means that the bounce frequency (synonymous with modulating frequency), which is presumed to depend on the potential at the radius where the trapping occurs (around r_s), will decrease as the plasma response decays. In order to obtain the bounce frequency in the response for a given voltage, a least squares fit of a decaying exponential is found for a given trace. This fitted

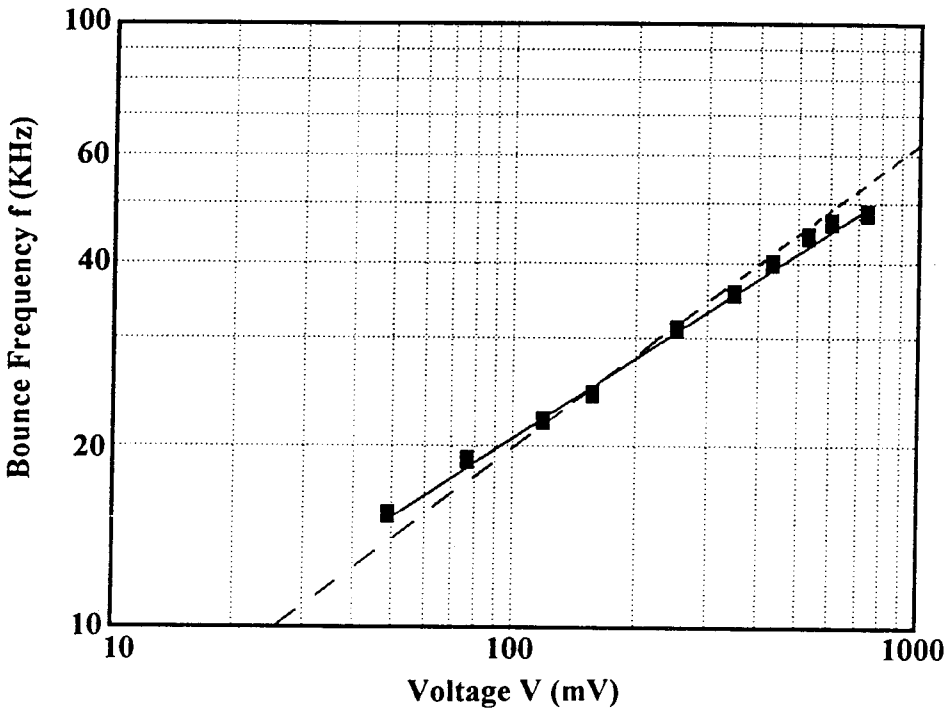

Figure 12. Bounce frequency, f, versus voltage, V, (applied voltage corrected for the decay) plotted on a log-log scale. Filled boxes correspond to data. Solid line is a least squares fit $f = AV^n$ where $n = 0.44$. Together with 21 other data sets, $n = 0.55 \pm 0.1$. Dashed lin shows a line where $n = 0.5$ for comparison.

exponential is then subtracted from the trace to obtain the modulation. The bounce frequency is then found by measuring the temporal distance between successive maxima. Using the decay rate of the fitted exponential, the applied voltage is corrected for decay to obtain the plasma potential resulting in the bouncing. A plot of the bounce frequency vs. the corrected applied voltage is shown in Figure 12. A least squares fit shows that the bounce frequency is given by $f = K_0 V^n$ where $n = 0.44$ and K_0 is a constant for this particular data set. Several other data sets were also obtained showing a similar behavior, giving a total of 22 sets of data where the bounce frequency could be measured. Identical fits were carried out on the other data sets also, and together with the present results, a value of $n = 0.55 \pm 0.1$ was obtained. This is extremely close to the theoretical value of 0.5 predicted for bounce motion as shown by the equation [9, 11]

$$\omega_b^2 = \frac{m^2 \phi(r_s)}{B r_s} \frac{d\omega_0(r)}{dr}\bigg|_{r=r_s}$$

where ω_b is the bounce frequency and $\phi(r_s)$ is the perturbed potential at the radius r_s, where the resonance condition $\omega = m\omega_0(r_s)$ is satisfied and around which trapping occurs.

It can be surmised that the modulation of the plasma response at larger applied voltages is caused by fluid element trapping within the potential well created by the $m = 2$ diocotron wave in the plasma. The idea of the potential well in the plasma is very similar to that of the Kelvin's cat's eyes in a plane parallel 2-D inviscid fluid with shear flow [12]. In the latter picture, a sinusoidal perturbation in the fluid results in closed contours of the streamlines, *in the frame moving with the perturbation*. A similar result is obtained in the plasma where the sinusoidally perturbed diocotron wave results in closed contours of the total potential, in the frame moving with the wave. The overall potential $\phi_1(r_s + \triangle r)$ around the radius r_s may be written as

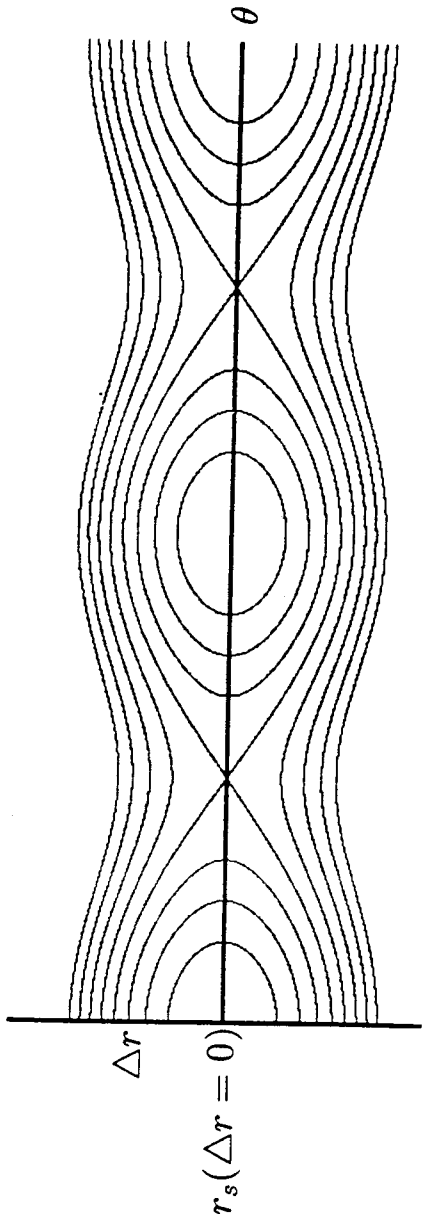

Figure 13. A plot of equi-potential contours in the plasma around the resonant radius r_s, when travelling with the wave speed ω/m. This is identical to the "cat's eyes" predicted by Kelvin (W. Thompson) in 1880 for the 2-D plane parallel flow of a inviscid incompressible fluid.

$$\phi_1(r_s+\triangle r)=\phi_0(r_s)+\left.\frac{d\phi_0}{dr}\right|_{r_s}\triangle r+\left.\frac{d^2\phi_0}{dr^2}\right|_{r_s}\frac{(\triangle r)^2}{2}+\cdots+K_1cos(m\theta-\omega t)$$

where the last term represents the perturbation and quantities with a zero subscript represent steady-state values. K_1 is an arbitrary constant. The steady-state electric field $E_{0r}(r_s)$ at the resonant radius will vanish when traveling with the wave speed $\omega/m=\omega_0(r_s)$ by virtue of the drift equation of motion (see Chapter 4). Neglecting higher order terms, the above equation then reduces to

$$\phi_1(r_s+\triangle r)=\phi_0(r_s)+\left.\frac{d^2\phi_0}{dr^2}\right|_{r_s}\frac{(\triangle r)^2}{2}+K_1cos(m\theta)$$

around r_s. It is apparent that contours of constant potential will form closed loops in the $(\triangle r,\theta)$ plane as shown in Figure 13, identical to the "cat's eyes" picture in reference [10]. These are closed contours of potential around the resonant radius when traveling with the wave speed. This means that a fluid elements at r_s will see other elements at $r<r_s$ traveling faster than them, and elements at $r>r_s$ traveling at a slower speed.

3.5 NEGATIVE ENERGY TEST

The previous experiment showed that the $m=2$ diocotron wave in the plasma is damped by means of a collisionless decay process. It was assumed that the wall electrode was a perfect conductor (made out of gold plated copper). It has been shown theoretically that an increase in the wall resistance would *decrease* the damping rate of the diocotron waves [9]. This is because diocotron waves are *negative energy* waves, meaning that the removal of energy from the wave would cause the wave amplitude to increase. This property has already been experimentally verified for the $m=1$ diocotron [13]. It would seem that the $m=1$ mode would be easily affected since the resonance occurs at the electrode wall and is undamped to begin with. But it is not so apparent that the $m=2$ diocotron should be affected at all, since it is already damped. If the $m=2$ diocotron

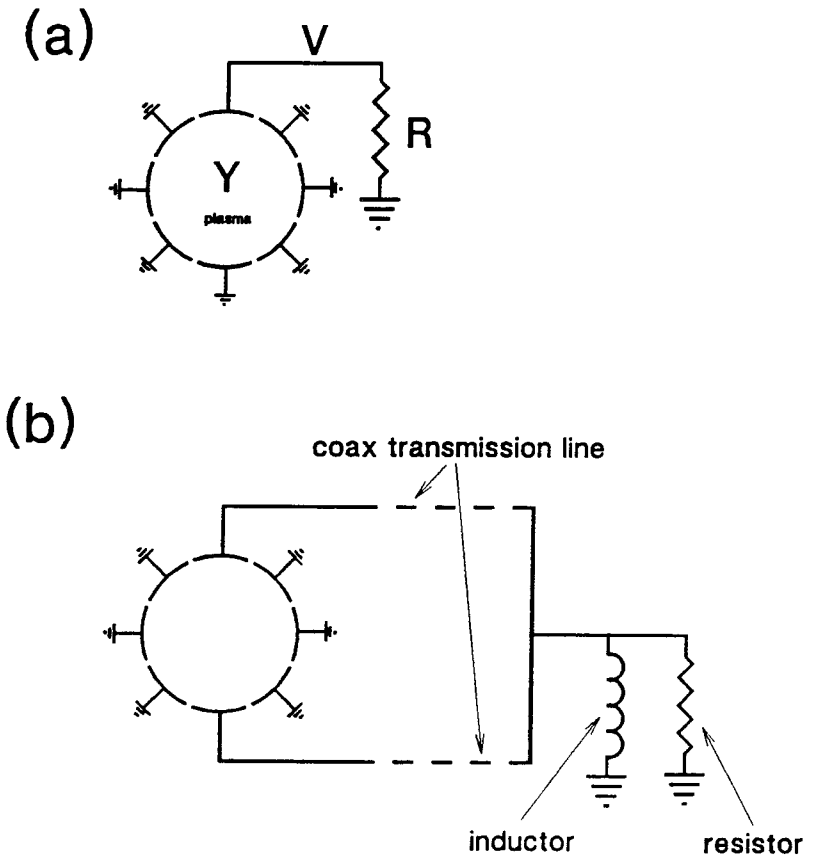

Figure 14 (a). Addition of an external resistor to an octupole sector that would decrease the wall conductivity seen by the diocotron wave inside the plasma. (b) A more practical setup for selectively allowing the $m = 2$ diocotron wave in the plasma experience a lower wall conductivity. The inductor in shunt with the resistor tunes out the capacitance of the coaxial transmission line that connects the octupole, in vacuum, to the resistor physically located at the vacuum flange.

wave is a negative energy wave, then the damping rate should decrease by the addition of resistors to the octupole section as shown in Figure 14(a).

Care must be taken while performing this experiment so that the $m = 1$ diocotron is not excited. If the $m = 1$ were excited, it would dominate the plasma response since it would now turn into an unstable growing mode. To avoid this, the resistor R is connected to opposite octupole sectors as in Figure 5(d). This ensures that no $m = 1$ current would be induced in the electrode, since their phasor sum would cancel out in the resistor.

Another factor which must be considered is the capacitance of the coaxial transmission line connecting the octupole sector to the terminals at the vacuum flange. At the $m = 2$ frequency, the lower capacitive reactance dominates over the resistance R. Hence an inductor is placed in shunt with R so as to tune out the transmission line capacitance at the $m = 2$ resonant frequency, as shown in Figure 14(b).

3.6 RESULT OF NEGATIVE ENERGY TEST

With the above modifications in the experimental setup, an $m = 2$ diocotron wave was excited, in the usual manner, while a resistor was connected to two octupole sectors as in Figure 14(b). The received signal was digitized and the damping rate was found by χ^2 fitting a damped sinusoid to the digitized signal. The experiment was repeated for different values of resistor R and a graph of damping rate vs. R was made. The result is shown in Figure 15. The solid line shows a least squares fit to the data shown with error bars. It is immediately apparent that the damping rate does decrease with increase in resistance. The linear decrease in the damping rate can be predicted by theory and is derived later in Chapter 5 (see equation 24). The exact slope of the decrease of decay rate with resistance depends on the density profile of the plasma, which could not be measured with the present experimental setup. If the resistance is high enough, Figure 15 predicts that the $m = 2$ diocotron can even become an unstable growing mode! Although no

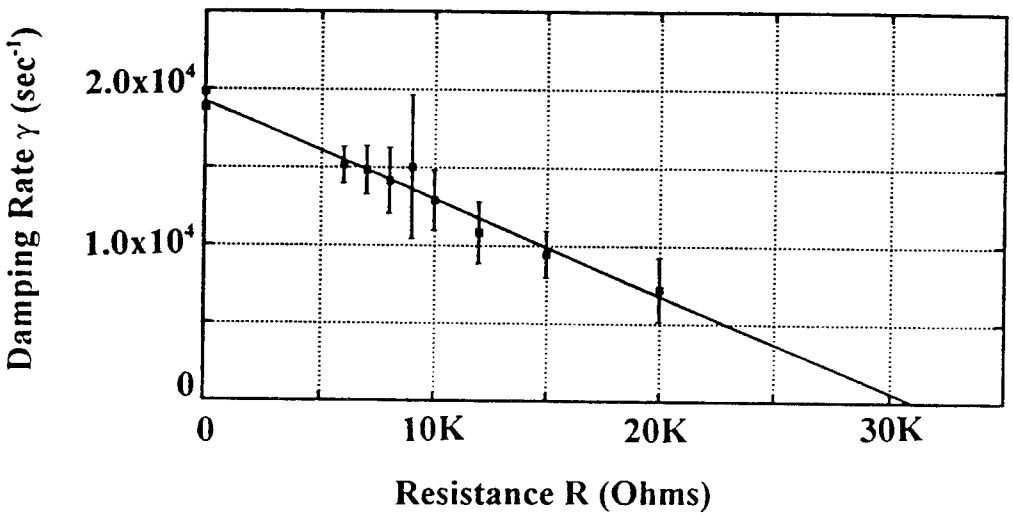

Figure 15. Decay rate of the $m = 2$ response versus resistance when a resistor R is connected to the wall electrode. Line is a least squares fit of the experimental data obtained from a large number of responses.

(a)

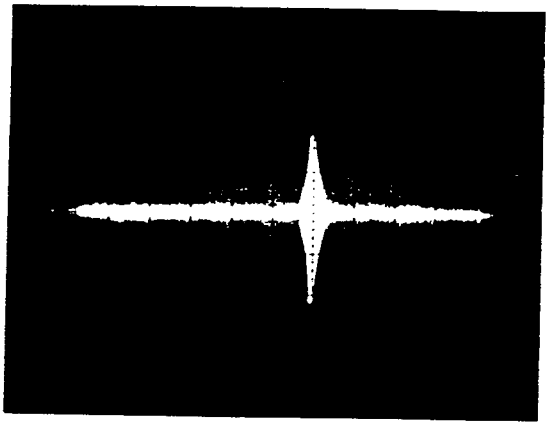

(b)

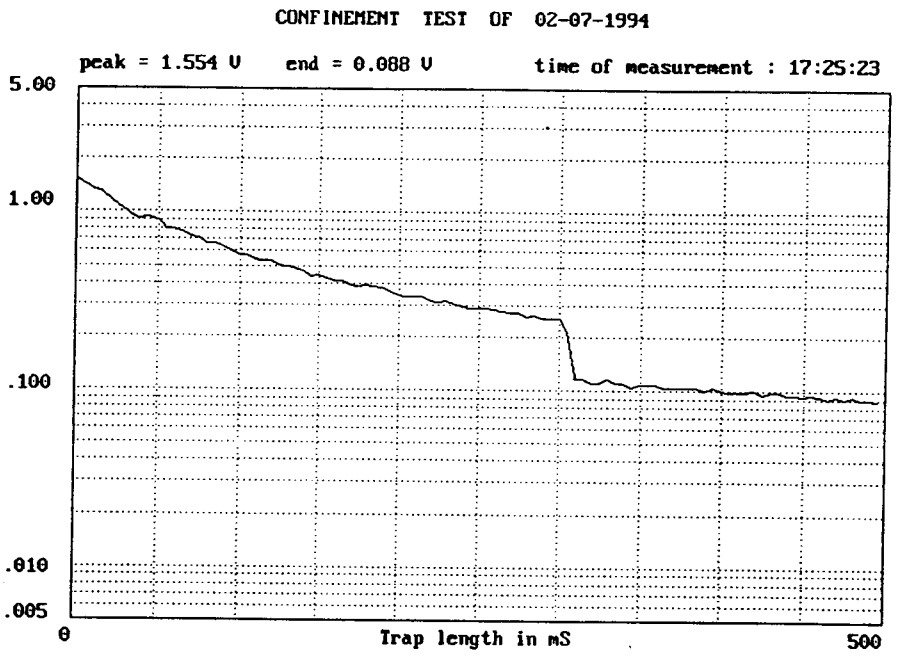

Figure 16. (a) Copy of the photograph of an oscilloscope trace showing an unstable (growing) $m = 2$ diocotron mode caused by the 386kΩ equivalent parallel resistance of a 1.5mH inductor ($Q = 94$) connected to an octupole sector. The frequency of the instability is about 320kHz. Voltage scale is 5V per division and time base is 50 ms per division. This shows that the instability occurs roughly around 300 ms after electrons are injected into the plasma trap. (b) A confinement plot taken at the same time as the photograph in (a). This shows that at the time that the $m = 2$ diocotron became unstable, particles were lost from the plasma.

experimental data was obtained to quantitatively measure a growth rate, unstable $m = 2$ diocotron modes have been observed qualitatively as in Figure 16(a). This is a copy of the photograph of an oscilloscope trace taken when an $m = 2$ diocotron was destabilized with the equivalent parallel resistance of a 1.5mH inductor. For this particular experiment, the $m = 2$ frequency was measured to be 320kHz. The equivalent parallel resistance of the inductor was measured to be 386kΩ at 350kHz, implying that the Q of the inductor is 94. Figure 16(b) shows the confinement plot when the $m = 2$ diocotron wave was destabilized. The sudden change in the confinement plot at 300ms occurs because the destabilized diocotron wave resulted in particle transport causing sudden loss of particles. After the loss of particles, the steady-state density profile must have changed and an unstable $m = 2$ diocotron no longer existed.

3.7 INTERPRETATION

As explained earlier, in the beginning of section 3.3, there is a low frequency resonance in the pure electron plasma. This induces a current in the wall of the electrode. Upon removal of the source of excitation, the plasma response decays. The negative energy test shows that the decay is not caused by any dissipative process at the wall. The time scale in which the response decays is much smaller than any collision time. Hence the diocotron resonance decays due to some collisionless non-dissipative decay process.

The collisionless decay predicted by the above experiments is not unique to pure electron plasma. The most famous example is that of Landau damping of plasma oscillations in neutral plasma, which also was experimentally verified to exhibit trapped particle oscillations [14 – 17].

Phase mixing is often a term used by researchers to describe Landau damping, and is very appropriate here also. Experimentally, what one observes is a decay of the induced current in the wall of the electrode. The induced current at the wall, and hence the electric field at the wall, is the result of integrating all the perturbations throughout all the radii in

the plasma. As Figure 9 shows, the angular velocity is different at different radii for monotonically decreasing density profiles, so the perturbations at different radii are convected at different rates - a shearing process. Hence the phasor sum of the perturbations at the wall may cause the electric field at the wall to decay.

REFERENCES

[1] J.S. deGrassie and J.H. Malmberg, Phys. Rev. Lett. **39**, 1333 (1977)

[2] J.S. deGrassie and J.H. Malmberg, Phys. Fluids **23**, 63 (1980)

[3] G. Mourier, in Crossed Field Microwave Devices, edited by E. Okress (Academic Press Inc., N.Y., 1961)

[4] A.H.W. Beck, Space Charge Waves and Slow Electromagnetic Waves (Pergamon Press, 1958)

[5] G.G. McFarlane and H.G. Hay, Proc. Phys. Soc. **63**, 409 (1953)

[6] H.F. Webster, J. Appl. Phys. **26**, 1386 (1955)

[7] R.L. Kyhl and H.F. Webster, IRE Trans. Electron Dev. **3**, 172 (1956)

[8] J.R. Pierce, IRE Trans. Electron Dev. **3**, 183 (1956)

[9] R.J. Briggs, J.D. Daugherty, and R.H. Levy, Phys. Fluids **13**, 421 (1970)

[10] B. Cluggish and C.F. Driscoll, Bull. Am. Phys. Soc. **38**, 1972 (1992)

[11] J.S. deGrassie, Ph.D. thesis, University of California, San Diego (1977)

[12] W. Thompson, Nature **23**, 45 (1880)

[13] W.D. White, J.H. Malmberg, C.F. Driscoll, Phys. Rev. Lett. **49**, 1822 (1982)

[14] L. Landau, J. Phys. (Moscow) **10**, 25 (1946)

[15] T.M. O'Neil, Phys. Fluids **8**, 2255 (1965)

[16] J.H. Malmberg and C.B. Wharton, Phys. Rev. Lett. **19**, 775 (1967)

[17] C.B. Wharton, J.H. Malmberg and T.M. O'Neil, Phys. Fluids **11**, 1761 (1968)

CHAPTER 4

DIOCOTRON THEORY

4.1 INTRODUCTION

The previous chapter showed that when the cylindrical column of pure electron plasma is excited with a particular frequency, much below the cyclotron frequency and having an $m = 2$ azimuthal symmetry, a resonance can be observed. The plasma responds to this excitation by inducing a current in the wall of the electrode. When the source of excitation is removed, the induced current at the wall decays exponentially in the linear regime due to a collisionless decay process. This motivates us to evolve a model characteristic equation for the pure electron plasma system and attempt to find a complex eigenvalue ω in this system. The sign of the imaginary part of ω should be such as to produce a damping and the real part would correspond to the unique frequency of the $m = 2$ resonance. The ratio of the real part of ω to the imaginary part is the "Q" of the resonance, to borrow a term from second order RLC electrical circuits. A previous fit of the imaginary part of ω between theory and experiment proved unsatisfactory, as the theoretical prediction deviated from experimental observation by two orders of magnitude [1].

The remainder of the chapter deals with the derivation of the model differential equation and its solution. All the discussions below assume that the plasma temperature is zero (cold fluid model) and the cylinder wall is a perfect conductor. A discussion of the negative energy aspects of the diocotron wave is deferred to the next chapter.

4.2 THE PLASMA MODEL

The pure electron plasma column can be considered as a cylindrical column of rotating fluid. The axial motion of the fluid is neglected and the column is assumed to be

an infinitely long cylinder. We can now concentrate our efforts on the 2-D dynamics in the (r, θ) plane. The electric field $\vec{E}$ is assumed to be electrostatic. Hence

$$\vec{E} = -\nabla\phi \tag{1}$$

where ϕ is the electrostatic potential. Substituting this into Gauss's law, we get Poisson's equation:

$$\nabla^2\phi = \frac{ne}{\epsilon_0} \tag{2}$$

where n is the density, e is the charge of the electron and ϵ_0 is the permittivity of free space. The equation for the fluid velocity, neglecting viscosity and temperature, takes the form

$$nm_e\frac{D\vec{v}}{Dt} = -ne\left(\vec{E} + \vec{v} \times \vec{B}\right)$$

where m_e is the electron mass, $\vec{v}$ is the velocity and $\vec{B} = B_0\hat{\mathbf{z}}$ is the steady state confining magnetic field in the axial direction. $\frac{D}{Dt}$ denotes the convective derivative. Since we are interested only in the average fluid velocity neglecting cyclotron motion and inertial effects, the above equation reduces to

$$\vec{E} + \vec{v} \times \vec{B} = 0$$

which is also known as the drift equation. Neglecting the inertial effects and cyclotron effects in the drift approximation is equivalent to assuming that $\omega_{pe}^2/\omega_c^2 \ll 1$. And this implies that the energy of the system is mainly electrostatic and very little is kinetic.

Solving for $\vec{v}$ we obtain

$$\vec{v} = \frac{\vec{E} \times \vec{B}}{B_0^2}. \tag{3}$$

Using (1) and the previous equation, it is easy to show that

$$v_r = \frac{-1}{B_0 r}\frac{\partial \phi}{\partial \theta} \text{ and } v_\theta = \frac{1}{B_0}\frac{\partial \phi}{\partial r}$$

from which we get $\nabla \cdot \vec{v} = 0$ and

$$\nabla \times \vec{v} = \nabla^2 \phi \hat{\mathbf{z}} = \frac{ne}{\epsilon_0}\hat{\mathbf{z}}.$$

Along with equation (2), these equations for the velocity are analogous to those of a 2-D inviscid incompressible fluid where the fluid vorticity is proportional to the plasma density and the fluid streamline function is proportional to the plasma potential [2, 3]. Hence the dynamics of the pure electron plasma are equivalent to those of a 2-D inviscid incompressible fluid. The continuity equation for the 2-D fluid system takes the form

$$\frac{\partial n}{\partial t} + \vec{v} \cdot \nabla n = 0 \tag{4}$$

because the fluid is incompressible.

Equations (2), (3) and (4) constitute the basic equations for the plasma dynamics in the (r, θ) plane, and form the model equations for discussion of diocotron waves in the pure electron plasma. The variables used above are split into steady-state and perturbed quantities in the following way

$$\begin{aligned}
\vec{E} &= \vec{E_0}(r) + \vec{E'}(r, \theta, t) \\
\vec{v} &= \vec{v_0}(r) + \vec{v'}(r, \theta, t) \\
n &= n_0(r) + n'(r, \theta, t) \\
\phi &= \phi_0(r) + \phi'(r, \theta, t)
\end{aligned}$$

where zero subscripts stand for steady-state quantities and the primed variables are perturbed quantities. Steady-state quantities are functions of only the radius, while all perturbed quantities are assumed to have azimuthal and temporal dependence of the form $e^{im\theta - i\omega t}$.

4.3 STEADY-STATE

From equations (2), (3) and (4), the steady-state equations of the plasma column will reduce to the following

$$\nabla^2 \phi_0(r) = \frac{n_0(r)e}{\epsilon_0} \tag{5}$$

$$v_{0\theta}(r) = -\frac{E_{0r}(r)}{B_0}$$

or

$$\omega_0(r) = \frac{1}{rB_0}\frac{d\phi_0}{dr} \tag{6}$$

where $\omega_0(r)$ is the radially dependent angular velocity. Using equations (5) and (6), it can be shown that

$$\frac{1}{r}\frac{d}{dr}(r^2\omega_0) = \frac{n_0 e}{\epsilon_0 B_0} \tag{7}$$

which provides the relation between angular velocity and steady-state density.

From the steady-state picture, it is seen that the radial dependence of the angular velocity and electrostatic potential are determined by the radial density profile. If the radial density were uniform, i.e. $n_0(r)$ were independent of r, then a plasma that fills the cylinder would have an angular velocity that is independent of radius. This is the so-called rigid rotor profile. Monotonically decreasing density profiles have monotonically decreasing angular velocity profiles.

4.4 PERTURBED MODEL

If we neglect second-order effects (product of primed variables), the linearized perturbed equation of continuity will be:

$$\frac{\partial n'}{\partial t} + \vec{v_0} \cdot \nabla n' + \vec{v'} \cdot \nabla n_0 = 0.$$

With perturbations in t and θ as $e^{im\theta - i\omega t}$, this equation can be further modified as follows:

$$-i\omega n'(r) + im\omega_0(r)n'(r) + v_r'(r)\frac{dn_0}{dr} = 0$$

giving

$$n'(r) = \frac{iv_r'(r)}{(m\omega_0(r) - \omega)}\frac{dn_0(r)}{dr}. \tag{8}$$

The perturbed equation for v_r' is given by

$$v_r' = \frac{-1}{rB_0}\frac{\partial \phi'}{\partial \theta} = -\frac{im}{rB_0}\phi'$$

and hence

$$n'(r) = \frac{m}{rB_0\Big(m\omega_0(r) - \omega\Big)}\frac{dn_0(r)}{dr}\phi'. \tag{9}$$

Substituting this into the perturbed form of Poisson's equation

$$\nabla^2\phi' = \frac{n'e}{\epsilon_0}$$

we get:

$$\nabla^2\phi' = \frac{me}{\epsilon_0 rB_0\Big(m\omega_0 - \omega\Big)}\frac{dn_0}{dr}\phi'$$

or expanding out the Laplacian operator:

$$\frac{d^2\phi}{dr^2} + \frac{1}{r}\frac{d\phi}{dr} - \left\{\frac{m^2}{r^2} + \frac{me}{\epsilon_0 B_0}\frac{\frac{dn_0}{dr}}{r[m\omega_0 - \omega]}\right\}\phi = 0. \tag{10}$$

The primes have been dropped. It is assumed that only variables with a 0 subscript are steady-state quantities. Equation (10) represents the variation of the perturbed potential in the plasma from the center ($r = 0$) up to the wall ($r = b$). In cases where the plasma edge ($r = a$) does not extend up to the wall (i.e. $a < b$), equation (10) is still valid within the plasma. In between the plasma and the wall, equation (10) will reduce to the simple form:

$$\frac{d^2\phi}{dr^2} + \frac{1}{r}\frac{d\phi}{dr} - \frac{m^2}{r^2}\phi = 0 \tag{11}$$

which is seen to be an equi-dimensional equation in ϕ, having the solution $\phi(r) = K_2 r^m + K_3 r^{-m}$, where K_2 and K_3 are arbitrary constants.

The form of equation (10) in rectangular coordinates is often referred to as the Rayleigh equation, or the Rayleigh-Kuo equation [4 – 8]. In this thesis, it will be referred to as the diocotron equation. With normalized units specified below, the diocotron equation may be written as

$$\frac{d^2\phi}{d\rho^2} + \frac{1}{\rho}\frac{d\phi}{d\rho} - \left\{\frac{m^2}{\rho^2} + \frac{2\frac{df(\rho)}{d\rho}}{\rho[g(\rho) - u]}\right\}\phi = 0 \tag{12}$$

where $\rho = r/b$ is the normalized radius, $f(\rho)$ is the normalized density with $f(0) = 1$, $g(\rho)$ is the normalized angular velocity with $g(0) = 1$, and $u = \omega/m\omega_0(0)$ is the wave speed ω/m normalized to the central rotation frequency $\omega_0(0)$. Use is made of the relation

$$\frac{1}{\rho}\frac{d}{d\rho}\left(\rho^2 g(\rho)\right) = 2f(\rho) \tag{13}$$

which follows from (7).

To obtain an eigenvalue, equation (12) should be solved for the homogeneous boundary conditions $\phi(\rho = 0) = \phi(\rho = 1) = 0$.

4.5 QUASIMODES

For a rigid rotor profile, equation (12) can be solved for all values of m. It has been shown that the eigenvalues for such a profile are [2]

$$\omega = \omega_0[m - 1 + \alpha^{2m}]$$

where $\alpha \equiv a/b$. This may be done by solving (12) with $df/d\rho = 0$ for $0 < \rho < \alpha$ and $\alpha < \rho < 1$ and then applying continuity of potential and jump in the electric field at

$\rho = \alpha$. This shows that all the eigenvalues for the constant density rigid rotor profile are real. Hence the diocotron waves for all m numbers are neutral modes of the system.

For the general case when $df/d\rho \neq 0$, equation (12) can be put into the form

$$\frac{d}{d\rho}\left[\rho^3(g-u)^2\frac{d\psi}{d\rho}\right] + (1-m^2)\rho(g-u)^2\psi = 0 \qquad (14)$$

by making the substitution $\phi = \rho(g-u)\psi$. For the $m = 1$, equation (14) is easily integrable and reveals $\phi(\rho) = K_4\rho\left[g(\rho) - u\right]$ as the only solution that is bounded at the origin. K_4 is an arbitrary constant. Applying the boundary condition at the wall shows that the $m = 1$ diocotron has a wave speed $u = g(1)$. Hence the $m = 1$ diocotron is an undamped wave (since the eigenvalue is real) with a frequency equal to the angular velocity at the wall ($\rho = 1$).

It has been shown that for a monotonically decreasing density profile, equation (12) has only one eigenvalue and that is for the $m = 1$, as we have seen [2, 9]. There are no eigenvalues (complex or real) for $m > 1$!

This leaves the explanation of the experimental results with a problem. Theory shows that there are no complex eigenvalues for the diocotron equation with a monotonically decreasing density profile, while the experiment suggests that we look for complex eigenvalues. This problem is overcome by realizing that the observed resonances are not normal modes, but quasimodes [9].

It will be shown below that a complex eigenvalue ω can be obtained by extending equation (12) to the complex ρ plane.

4.6 SOLVING THE DIOCOTRON EQUATION

Discussed below is the method for obtaining an eigenvalue of the complex form of (12) for the parabolic density profile $f(\rho) = 1 - \rho^2$ with the plasma extending all the way up to the wall (that is $\alpha = 1$).

Using equation (13), we find that when $f(\rho) = 1 - \rho^2$, $g(\rho) = 1 - \frac{\rho^2}{2}$. This shows that the normalized angular velocity varies between unity at the center ($\rho = 0$) and 0.5 at the wall ($\rho = 1$). Substituting for $f(\rho)$ and $g(\rho)$ in (12):

$$\frac{d^2\phi}{d\rho^2} + \frac{1}{\rho}\frac{d\phi}{d\rho} - \left\{\frac{m^2}{\rho^2} - \frac{4}{1 - \frac{\rho^2}{2} - u}\right\}\phi = 0$$

or

$$\frac{d^2\phi}{d\rho^2} + \frac{1}{\rho}\frac{d\phi}{d\rho} - \left\{\frac{m^2}{\rho^2} + \frac{8}{\rho^2 - [2(1-u)]}\right\}\phi = 0$$

or

$$\frac{d^2\phi}{d\rho^2} + \frac{1}{\rho}\frac{d\phi}{d\rho} - \left\{\frac{m^2}{\rho^2} + \frac{8}{\rho^2 - \rho_0^2}\right\}\phi = 0 \tag{15}$$

where $\rho_0 = \sqrt{2(1-u)}$. It is now a simple matter to solve equation (15) subject to homogeneous boundary conditions for $\phi(\rho)$.

Equation (15) has two regular singular points: one at the origin, $\rho = 0$, and the other at $\rho = \rho_0$ (singularities outside range $[0, 1]$ are neglected). Frobenius expansion around $\rho = 0$ gives:

$$\phi_1(\rho) = K_5\rho^m\left\{1 - \frac{2}{3}\left(\frac{\rho}{\rho_0}\right)^2 - \frac{1}{12}\left(\frac{\rho}{\rho_0}\right)^4 - \frac{1}{30}\left(\frac{\rho}{\rho_0}\right)^6 - \frac{13}{20}\left(\frac{\rho}{\rho_0}\right)^8 - \ldots\right\} \tag{16}$$

where K_4 is an arbitrary constant. The above expansion represents the only bounded solution at the origin, and is valid for $\left|\frac{\rho}{\rho_0}\right| < 1$. Around the singularity ρ_0, a similar expansion reveals two solutions $w_1(z)$ and $w_2(z)$ where $z = (\rho - \rho_0)/\rho_0$. One is analytic and the other has a logarithmic singularity:

$$w_1(z) = z + \frac{3}{2}z^2 + \left[\frac{m^2+2}{6}\right]z^3 - \left[\frac{m^2-1}{36}\right]z^4 + \left[\frac{m^4+m^2-15}{120}\right]z^5 + \ldots$$

$$p(z) = 1 + \left[\frac{m^2-24}{2}\right]z^2 - \left[\frac{13m^2+43}{18}\right]z^3 + \left[\frac{9m^4-173m^2-54}{216}\right]z^4 + \ldots$$

$$w_2(z) = 4w_1(z)ln(z) + p(z). \tag{17}$$

The solution for the perturbed potential, valid for $0 < |\rho| \leq 1$, is given by

$$\phi_2(z) = C_1 w_1(z) + C_2 w_2(z). \tag{18}$$

Equations (16) and (18) are the representations of the solutions of (15) in the different regions. Finding a $\phi(\rho)$ valid for all $|\rho| \leq 1$ lies in finding the values of the complex constants ρ_0, C_1 and C_2 so as to satisfy the boundary conditions and, in addition, the following:

$$\phi_1(\rho_x) = \phi_2(\rho_x) \tag{19}$$

and

$$\left.\frac{d\phi_1}{d\rho}\right|_{\rho=\rho_x} = \left.\frac{d\phi_2}{d\rho}\right|_{\rho=\rho_x} \tag{20}$$

for some ρ_x in the range $0 < \rho_x < \rho_0$. Equations (19) and (20) ensures that the solution to (15) has continuous potential and electric field variations for all $|\rho| \leq 1$. We thus have three conditions to determine C_1, C_2 and ρ_0 which will allow us to fix $\phi(\rho)$ to within a constant of proportionality, since the constant K_5 in (16) is not evaluated. Determining ρ_0 will give us the complex value of ω to determine the frequency and damping of a diocotron wave of azimuthal eigen number m.

The location of ρ_0 in the complex ρ plane depends on whether the quasimode is unstable or stable. Unstable diocotron $\Rightarrow$ Im(ω) $> 0 \Rightarrow$ Im(u) $> 0 \Rightarrow$ Im(ρ_0) < 0. Hence ρ_0 will be located in the fourth quadrant of the complex ρ plane if the resonance is unstable. On the other hand, if the resonance is damped (stable), then ρ_0 will lie in the first quadrant. In either case, the logarithmic singularity in equation (19) causes $\rho = \rho_0$ to be a branch point in the ρ plane. There will be a branch cut extending from $\rho = \rho_0$ to infinity as shown in Figure 17(a) and 17(b). The location of ρ_0 for a growing diocotron quasimode is shown in Figure 17(a). In such a case, evaluation of $z = (\rho - \rho_0)/\rho_0$ is straightforward.

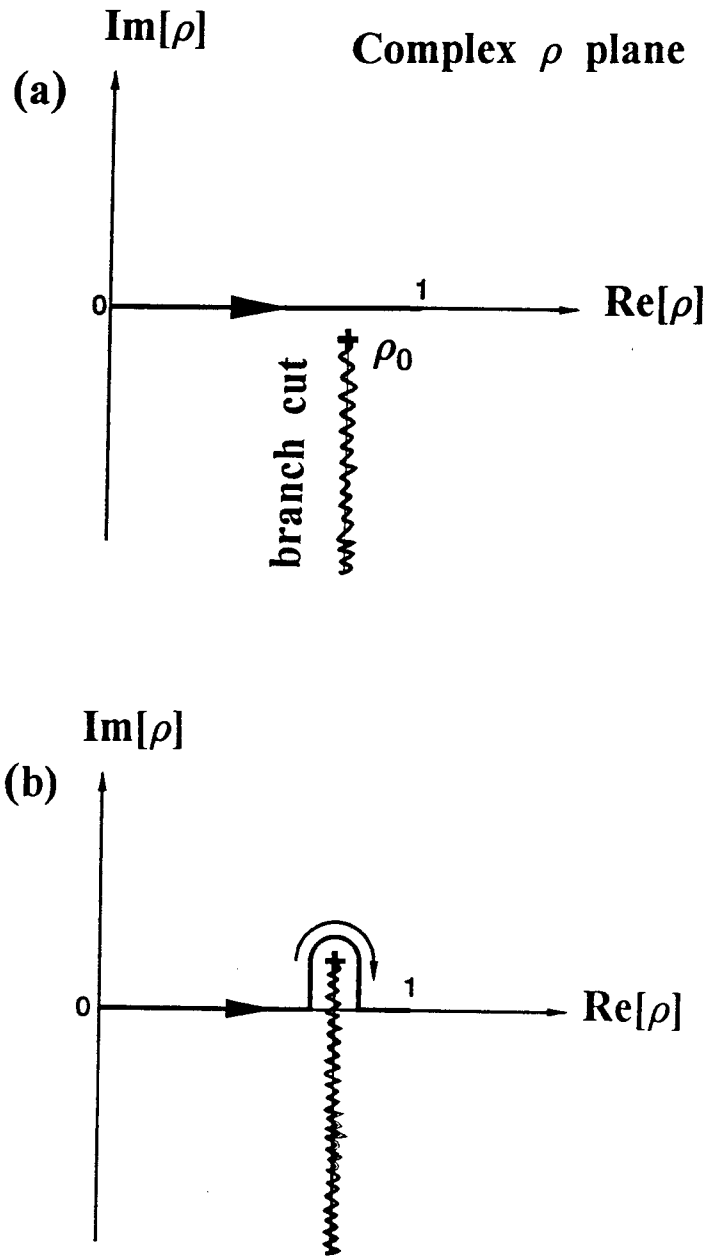

Figure 17. (a) Location of ρ_0 and the path of integration for the case of a temporally growing diocotron wave. (b) In the case of a temporally damped diocotron wave, ρ_0 is located in the first quadrant and the branch cut extends to infinity. The path of integration has to go around the branch point to remain on the same Reimann sheet and satisfy the boundary conditions.

However, when $\mathrm{Im}(\rho_0) > 0$, the path of integration (or continuous variation of ρ from 0 to 1) must be curved as shown in Figure 17(b), to avoid passing through the branch cut nd getting into a different Riemann sheet. If this method is followed in evaluating $z = (\rho - \rho_0)/\rho_0$ in equation (18), then equation (15) can be solved subject to the homogeneous boundary conditions. The resulting value of ρ_0 is then an eigenvalue of (15) for complex ρ.

4.7 RESULT

A computer program was used to evaluate $\phi_1(\rho)$ and $\phi_2(\rho)$ using the expansions shown above with 500 terms. The value of ρ_0 was varied iteratively to satisfy the boundary conditions and equations (19) and (20). It was found that for an $m = 2$ perturbation in a parabolic density profile, $\rho_0 = 0.9685 + i0.02199$. This corresponds to $\omega/\omega_0(b) = \omega_2 - i\gamma_2 = 2.1252 - i0.0852$. The $m = 2$ frequency has been scaled to the wall frequency of $\omega_0(b)$. The ratio of the real part of the eigenvalue to the imaginary part is $\frac{\omega_2}{\gamma_2} = \frac{2.1252}{0.0852} = 25$, and is twice the Q of the diocotron resonance. Hence for the parabolic profile $Q = \frac{\omega_2}{2\gamma_2} = 12.5$. Using the same program, the $m = 1$ diocotron has the values $\omega/\omega_0(b) = 1 + i0$. In other words, the $m = 1$ diocotron is an undamped mode with the frequency equal to the wall frequency, as predicted by theory.

The method of solving the diocotron equation by Frobenius expansion, as outlined above, is by no means unique. It has been shown that the solutions of (12) for the general family of profiles $f(\rho) = (1 - \rho^{2p})$, where p is a positive integer, can be expressed in terms of hypergeometric functions [9]. Chapter 5 discusses another method for obtaining the frequency and damping rate of the diocotron waves. For the $m = 2$ diocotron wave in the parabolic profile $f(\rho) = 1 - \rho^2$, the result obtained by these three different methods (Frobenius expansion of the complex equation, hypergeometric functions and numerical solution discussed in Chapter 5) all agree.

Does this fit the experimental observations? Our experimental setup cannot measure the steady-state density profile of the plasma. Hence, it is not possible to predict the exact $m = 2$ frequency and decay rate for a practical density distribution. However, it is possible to compare the Q of the resonance obtained experimentally and theoretically. The Q observed experimentally is $Q = 42$. The above theory predicts $Q = 12.5$, less than one-third of the experimental value. However, this is a much closer agreement between theory and experiment than the previous model [1]. The next chapter will reveal that the difference seen in our case may be attributed to the lack of knowledge about the steady-state density profile that exists in the experiment. In fact, it will be shown that the diocotron resonances and the Q are dependent on the density profiles. A value of Q equal to the experimental value of 42 can be obtained by a profile which is smoother at the plasma boundary and which does not extend all the way upto the wall.

4.8 SUMMARY

To recapitulate the theoretical result: a linear mathematical model for the perturbed potential in the pure electron plasma was derived using the Poisson's, drift and continuity equations. This equation (the diocotron equation) has singularities for real values of the wave frequency ω that lie within the range of angular velocities of the plasma. Previous theoretical work has shown that there are no eigenvalues for the case when $m > 1$ in a plasma with a monotonically decreasing density profile. The diocotron equation was solved using Frobenius expansion by extending the independent variable ρ to the complex domain. This method of solution, for an $m = 2$ disturbance in the particularly simple parabolic density profile, revealed the existence of a complex eigenvalue that indicates that the $m = 2$ diocotron wave in the parabolic density profile is damped. Moreover, there is a unique frequency associated with it. All this, without *any* assumption of collisions or other such dissipative mechanisms to explain the damping! In

other words, the linear model predicts a unique frequency of propagation and a non-dissipative decay process.

The ratio of the wave frequency to the damping rate, the Q of the resonance, is within about one-third of the experimentally observed Q. This is a much closer agreement than the previous model.

REFERENCES

[1] J.S. deGrassie, Ph.D. thesis, University of California, San Diego (1977)

[2] R.J. Briggs, J.D. Daugherty, and R.H. Levy, Phys. Fluids **13**, 421 (1970)

[3] C.F. Driscoll and K.S. Fine, Phys. Fluids B **2**, 1359 (1990)

[4] H.L. Kuo, J. Meteor. **6**, 105 (1949)

[5] L.P.J. Kamp, J. Phys. A: Math. Gen. **24**, 2029 (1991)

[6] L.P.J. Kamp, Europhys. Lett. **20**, 217 (1992)

[7] S.J. Rosecrans and D.H. Sattinger, J. Math. Phys. **45**, 289 (1966)

[8] E.G. Broadbent and D.W Moore, Proc. Royal Soc. London A **384**, 1 (1982)

[9] N.R. Corngold, Phys. Plasmas **2**, 620 (1995)

CHAPTER 5

COMPUTATIONAL RESULTS

5.1 INTRODUCTION

The previous chapter outlined a way of solving the diocotron equation by the brute force method of Frobenius expansion for the particularly simple parabolic density profile. Although this example showed clearly the existence of an eigenvalue for the complex form of the diocotron equation, the value of Q obtained did not correlate exactly with experiment. It is highly probable that the plasma has a density profile different from the parabolic one. Moreover, the parabolic profile is not smooth at the plasma edge, and perhaps the profile smoothness affects the resonant frequency and damping rate of the diocotron wave. This motivated us to solve the diocotron equation for other less simple density profiles. One stumbling block was the amount of tedious numerical hand calculations required for one profile. Other profiles would involve more calculations because of their complexity. A less tedious alternative to Frobenius expansion was required, and this was found in the form of numerical solution of the diocotron equation using the Runge-Kutta technique and run on a computer.

Equation (12), the normalized diocotron equation which is more amenable to numerical calculations, is reproduced below:

$$\frac{d^2\phi}{d\rho^2} + \frac{1}{\rho}\frac{d\phi}{d\rho} - \left\{ \frac{m^2}{\rho^2} + \frac{2\frac{df(\rho)}{d\rho}}{\rho[g(\rho) - u]} \right\}\phi = 0.$$

It is immediately apparent that this method would also have problems at the resonant radius where $u = g(\rho)$. This is overcome by using a slight positive imaginary part for u while doing the calculations. Next question is: what value of u should be used? This is where the method of solving by a computer seems more attractive. It is possible to solve

(12) for different values of Re(u) ranging from, say -20 to $+20$, normalized to the central rotation frequency. The advantage is that one can obtain all possible frequencies where the diocotron resonance may occur, if at all it occurs at more than one frequency. There is a more powerful reason involved and that is discussed in the next section.

5.2 ELECTRICAL MODEL

In the experiment described in chapter 3, we observed the plasma response to a short pulse. The pulse was in the form of a voltage applied to an octupole section, and the response was a current induced in the electrode. This may be represented by the circuit diagram of Figure 18(a). If $V(\omega)$ and $I(\omega)$ represent the Fourier transforms of the voltage and current respectively, then $I(\omega) = V(\omega)/Z(\omega)$ or $I(\omega) = V(\omega)Y(\omega)$ where $Y(\omega)$ is the *plasma admittance function*. In the limit that the applied voltage pulse is a delta function, $V(\omega) = 1$ and $I(\omega) = Y(\omega)$. Then the inverse Laplace transform of $Y(\omega)$ becomes the *impulse response* of the plasma. If $V(\omega) \neq 1$ then $Y(\omega) = I(\omega)/V(\omega)$, i.e. the plasma admittance is the ratio of the current to the voltage. It is shown in the appendix that $Y(\omega)$ may be written as

$$Y(\omega) \equiv \frac{I(\omega)}{V(\omega)} = i\omega\left(\epsilon_0 \frac{L}{2\pi}\right)\left(\frac{E_\rho(\rho,\omega)}{\phi(\rho,\omega)}\bigg|_{\rho=1}\right)\left(\frac{l}{L}\right)^2 \sin^2\left(\frac{m\pi}{8}\right)$$

i.e.
$$Y(\omega) = i\omega AC(\omega)F^2 \tag{21}$$

where
$$C(\omega) = \frac{E_\rho(\rho,\omega)}{\phi(\rho,\omega)}\bigg|_{\rho=1}$$

$F = \sin(m\pi/8)$, an angular form factor, and $A = l/L$ is a length form factor. $C(\omega)$ may be considered as a frequency dependent "capacitance function" since (21) has the form of a capacitive susceptance and $AC(\omega)$ has the dimensions of capacitance. Thus the linear behavior of the plasma to an applied pulse may be found by essentially calculating $C(\omega)$.

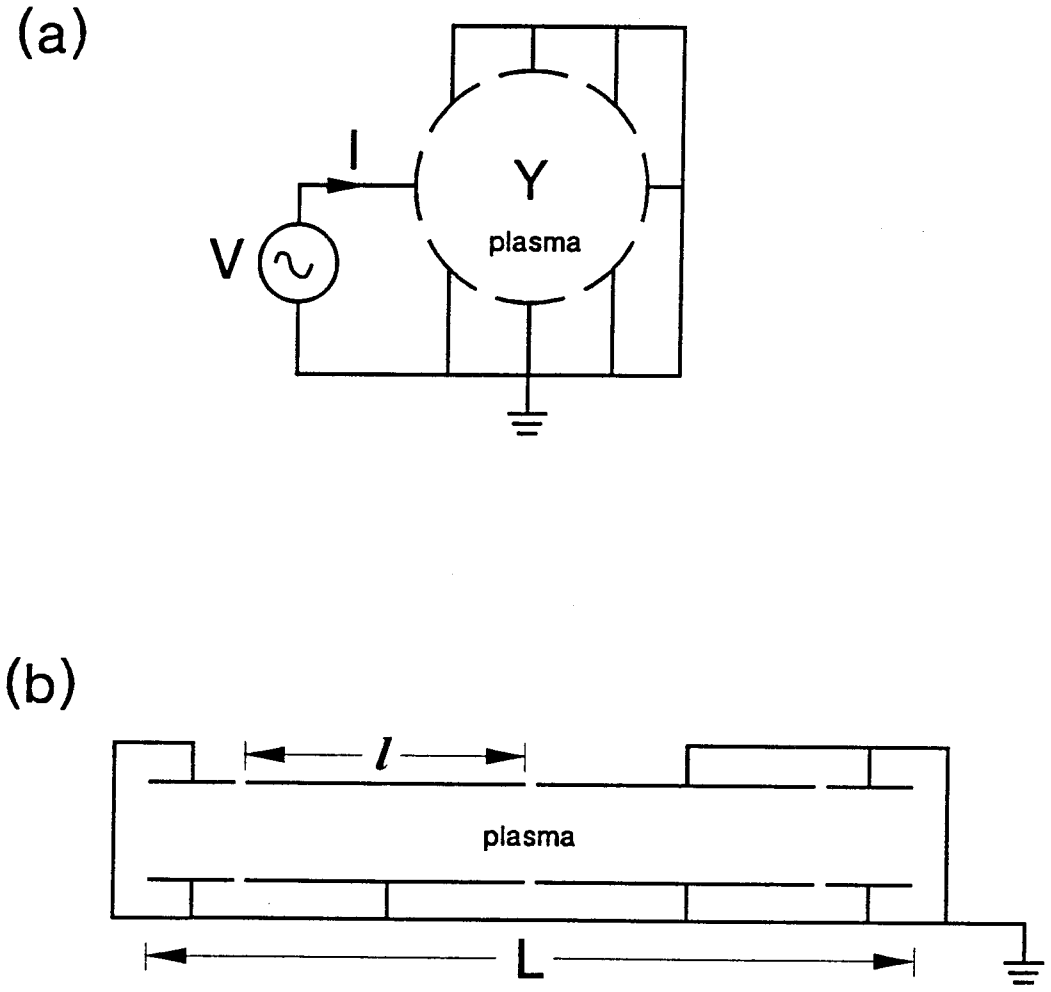

Figure 18. (a) Circuit diagram representation of the experimental setup for observing the diocotron resonance. The cross section of the plasma is shown. The octupoles tend a 45 degree angle at the center of the cylinder. Only one sector of the octupole is used for exciting the plasma. If additional sectors were used, say in an $m = 2$ configuration, $Y(\omega)$ would be changed only by numerical factors. (b) The axial schematic of the plasma (neglecting end effects) showing that only one octupole sector is used to excite and receive the plasma.

The method of calculation is as follows. For a plasma with a given $f(\rho)$ and $\alpha = a/b$, the response for a given m is found by solving (12) for $\phi(\rho = 1)$ and $E_\rho(\rho = 1)$ for a certain wave speed u. This gives the $C(\omega)$ for that frequency $\omega = mu\omega_0(0)$. The wave speed is then incremented by a small step size and the calculation is repeated. By repeating this process, it is possible to calculate $C(\omega)$ for a wide enough range of frequencies that allows us to calculate the discrete inverse Fourier transform of $C(\omega)$. It will be shown below that the response of the plasma is essentially the inverse Fourier transform of $C(\omega)$. That is to say, it is possible to simulate the experiment numerically to obtain the linear response. And one can do this for any possible profile.

5.3 DETAILS OF THE NUMERICAL METHOD

A program was written to find $C(\omega)$ for selective density profiles. A useful representation of a density profile for numerical work is that of a polynomial in the normalized radius ρ, with the density smooth at the origin and decreasing monotonically with ρ (the study of non-monotonic density distributions is beyond the scope of this research). Hence the simplest $n_0(\rho)$ would be the parabolic distribution $f(\rho) = 1 - \rho^2$ discussed in the previous chapter. More complicated cases are obtained by including more terms in higher powers of ρ. It was decided to include only even powers of radius. The coefficient of higher powers may be obtained by imposing conditions at the plasma edge to make the profile more smooth when $f(\rho) = 0$. We can thus obtain the profiles listed in Table 4. The primes indicate differentiation with respect to ρ. For the case when the plasma does not extend all the way to the wall (i.e. $\alpha < 1$), the profiles are modified so that $\rho \rightarrow \rho/\alpha$, and equation (12) is solved only to $\rho = \alpha$. In such cases, the field at the wall is obtained by solving the normalized form of equation (11) for $\alpha \leq \rho \leq 1$ with continuity in $\phi(\rho = \alpha)$ and $\phi'(\rho = \alpha)$. The last column in the Table 4, file name, is used to distinguish the various results in Plates 1-5. The eigen number would be substituted for m

$f(\rho)$	profile name	smoothness at $\rho = \alpha$	file name
$1-\rho^2$	simple power two	not smooth	*m*te0x
$1-2\rho^2+\rho^4$	power two (#1)	$f'(\alpha)=0$	*m*te1x
$1-3\rho^2+3\rho^4-\rho^6$	power two (#2)	$f'(\alpha)=f''(\alpha)=0$	*m*te2x
$1-\rho^4$	simple power four	not smooth	*m*fe0x
$1-3\rho^4+2\rho^6$	power four (#1)	$f'(\alpha)=0$	*m*fe1x
$1-6\rho^4+8\rho^6-3\rho^8$	power four (#2)	$f'(\alpha)=f''(\alpha)=0$	*m*fe2x
$1-\rho^6$	simple power six	not smooth	*m*se0x
$1-4\rho^6+3\rho^8$	power six (#1)	$f'(\alpha)=0$	*m*se1x
$1-10\rho^6+15\rho^8-6\rho^{10}$	power six (#2)	$f'(\alpha)=f''(\alpha)=0$	*m*se2x

Table 4. The normalized steady-state density profiles $f(\rho)$ that are used in the computational work. First column is the representation of the $f(\rho)$ as a polynomial in ρ, while the second column indicates the name. The third column shows the conditions imposed on the profile at the edge ($\rho = \alpha$) to obtain the coefficients (in addition to the condition that $f(\rho = 1) = 0$). Fourth column gives the short file names that are referred to in Plates 1-5.

and x would be substituted by the value of α times 100. For example, the result for an $m = 2$ perturbation in a power six (#2) profile with $\alpha = 0.80$ would have a file name of 2se280.

The use of a non-zero imaginary part for u in solving (12) will result in a slightly higher damping. This may be compensated for in the inverse Fourier transform by multiplying the end result with a term like $e^{\sigma t}$ where σ is proportional to the imaginary part of u. But in comparing $C(\omega)$ for different profiles and to model $C(\omega)$ accurately, the positive imaginary part of u used should be neither too large nor too small. A large value for Im[u] results in an incorrect $C(\omega)$. To avoid numerical errors, it should be greater than the maximum value of $dg/d\rho$. A value equal to 1/10 of the frequency step size was used for Im[u].

When computing $C(\omega)$, the vacuum capacitance of the electrode structure would be included. In order to concentrate only on the effects of the plasma, this vacuum capacitance has been subtracted out from the computed $C(\omega)$.

5.4 RESULTS

Using the techniques described above, equation (12) was used to find $C(\omega)$ for the various profiles listed and various azimuthal eigen numbers. Figure 19(a) shows the real and imaginary parts of the capacitance function for $m = 2$ quasimode for a simple power two profile. The two marks on the central horizontal line in Figure 19(a) indicate the central angular velocity and plasma edge velocity. In this case, where $\alpha = 1$, the plasma edge angular velocity is the same as $g(1)$, or the angular velocity at the wall. It is apparent that $C(\omega)$ becomes significant only when u lies in the range of the angular velocities of the plasma. Moreover, $C(\omega)$ is more significant for the range of angular velocities near the plasma edge than near the center. The shape of the function seems to suggest that $C(\omega)$ can be approximated as a Lorentz function, or a simple complex pole:

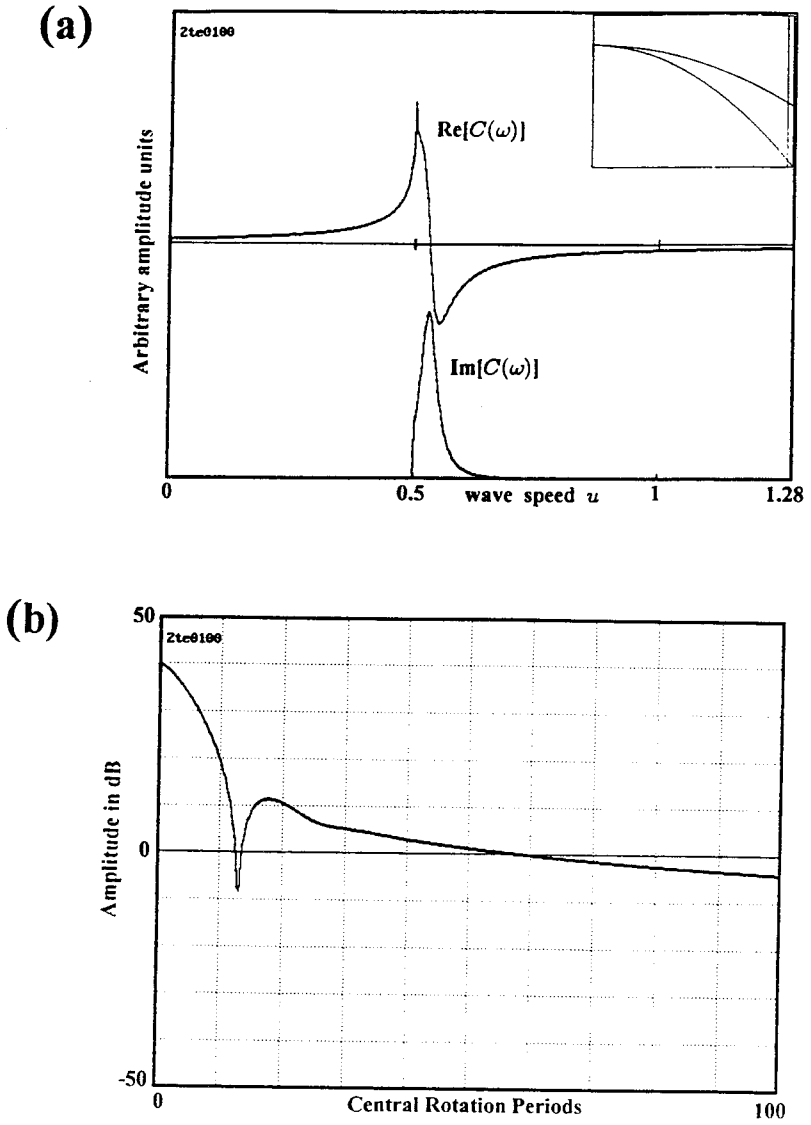

Figure 19. (a) A plot of $C(\omega)$ for the simple power two profile with $\alpha = 1$. The real part is shown on top and the imaginary part is shown just below it. The common x-axis is the wave speed u as it varies from 0 at the far left to 1.28 on the far right. The range of normalized angular velocities for the plasma lies between the two marks on the central horizontal line. For this profile, the normalized rotation frequency at the plasma edge, $g(\rho = 1) = 0.5$. (b) The magnitude of the inverse Fourier transform of $C(\omega)$, plotted on a semilog scale. Time is measured in terms of the central rotation periods. This is the response of the plasma to a delta function in voltage applied at the octupole sector. For this particular profile, the temporal response is non-exponential with an asymptotic algebraic decay.

$$C(\omega) = \frac{B}{\omega - [\omega_2 - i\gamma_2]} \tag{22}$$

where ω_2, γ_2 (> 0) and B (< 0) are found by fitting the model to the figure. Using this in (21), the admittance of the plasma would appear to be that of a simple complex pole. For this form of $C(\omega)$, the inverse Fourier transform of $Y(\omega)$ is essentially that of $C(\omega)$ except for a constant term. This constant term would correspond to the contribution of the vacuum electrode structure (without the plasma) to the inverse transform. The result of this constant term is that when a delta function in voltage is applied, a delta function in current is obtained in the time domain. Otherwise, the effect of the plasma is contained in the inverse transform of $C(\omega)$. Using the above model and comparing with Figure 19(a), it is seen that ω_2 corresponds to the wave speed where $\mathrm{Re}[C(\omega_2)] = 0$. And γ_2 is given by:

$$\gamma_2 = \frac{\omega_h - \omega_l}{2}$$

where ω_h and ω_l are the angular frequency points where $\mathrm{Im}[C(\omega)]$ falls to half its peak value. In a manner of speaking, γ_2 corresponds to the width of $\mathrm{Im}[C(\omega)]$. For the simple power two profile, $\omega_2 = 2.12$ and $\gamma_2 = 0.106$ normalized to the frequency $g(1)$. This roughly corresponds, within the bounds of numerical error, to the complex eigenvalue obtained in Chapter 4 by solving equation (15) using Frobenius expansion. The higher damping obtained by the computational method may be accounted for by the use of a positive imaginary part of u, which should result in higher damping.

The inverse transform of $C(\omega)$ is shown in Figure 20. This is really an inverse Laplace transform since ω has a slight positive imaginary part. As expected from the model equation (22), the transient response of the plasma to a delta function is a decaying sinusoid. The frequency of the sine wave is ω_2 and the initial decay rate should correspond to γ_2. These ideas are intuitively inferred from Figure 19(a). The angular frequency (and hence radius) where $\mathrm{Re}[C(\omega)] = 0$ is the resonant frequency (resonant radius) of the diocotron wave and the width of $\mathrm{Im}[C(\omega)]$ corresponds to the decay rate of the temporal

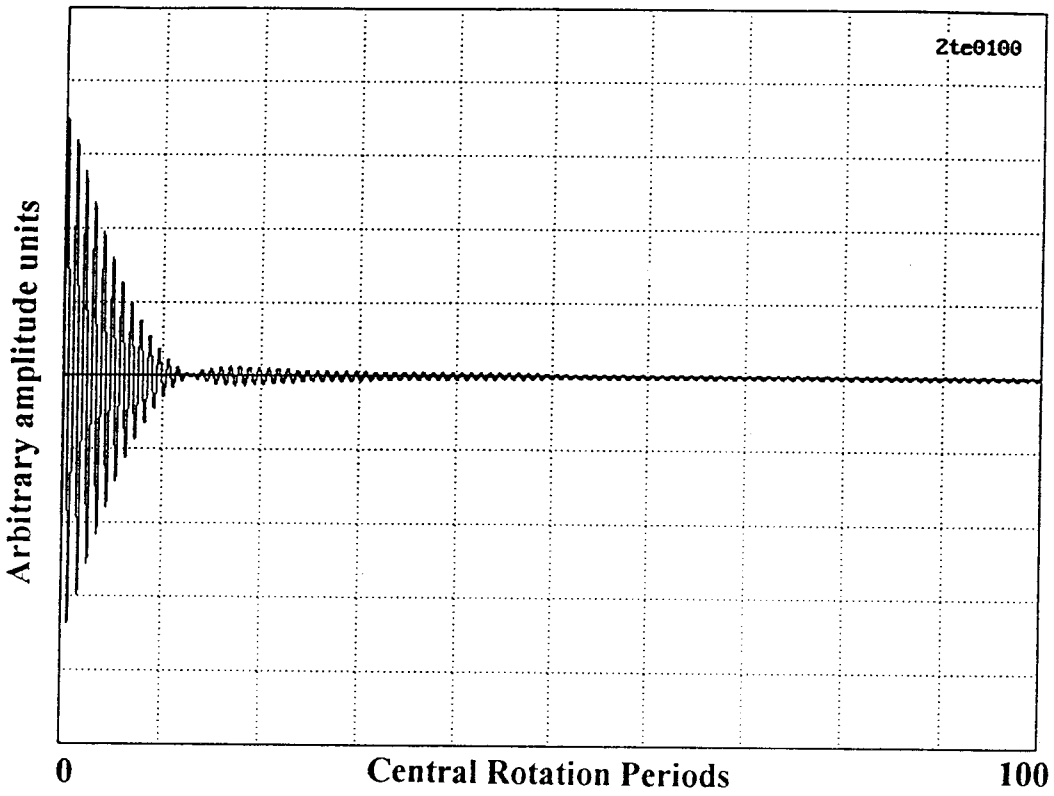

Figure 20. The inverse Fourier transform of the capacitance function of a plasma with a simple parabolic profile with $\alpha = 1$ and $m = 2$. The initial response corresponds to a fast decay. However, the asymptotic behavior corresponds to an algebraic decay.

response. From Figure 20, it is apparent that there is more happening to the transient response than a simple exponential decay. It can be seen that after the response decays away, the amplitude rises again, and then persists for a long time. This behavior is brought out in a better way by observing the magnitude of the transient response plotted on a semilog scale as in Figure 19(b). It is immediately apparent that the decay is not at all a simple exponential process. There is an initial fast decay followed by a sudden dip in the magnitude, and then an asymptotic algebraic decay. The magnitude of the inverse Fourier transform of a simple pole would leave a straight line trace on a semilog graph. It is seen from Figure 19(a) that the simple pole model of $C(\omega)$ is a rough approximation. Both the real and imaginary parts of the capacitance function are not symmetric about the resonant frequency. This asymmetry is heightened in the plot of Im$[C(\omega)]$. The part of Im$[C(\omega)]$ very near the plasma edge is very abruptly cut off. It is speculated that this asymmetry of $C(\omega)$ is responsible for the nature of the response shown in Figure 19(b).

The slow asymptotic decay of the diocotron wave was actually predicted by Case for perturbations occurring in planar Couette flow [1]. Since the model is the same for either systems (with exception of the geometry), it is reasonable to assume that the algebraic decay should occur for the diocotron waves also.

The question arises as to how much of the results of Figure 19 are unique to the profile that was considered. And how much of it is due to the particular value of the azimuthal eigen number? To answer these questions, $C(\omega)$ was calculated for different profiles and m numbers. Plates 1-5 show the result of these calculations. They show $C(\omega)$ and its inverse transform (magnitude only) next to it. The inverse transforms are all plotted on the same amplitude and time scales (same as in Figure 19(b)), while all the $C(\omega)$ are plotted on the same horizontal scale for the wave speed. The central angular velocities for all profiles are normalized to one. However, the edge angular velocity $g(\alpha)$ and the wall angular velocity $g(1)$ are profile dependent. Marks are made on the central horizontal line

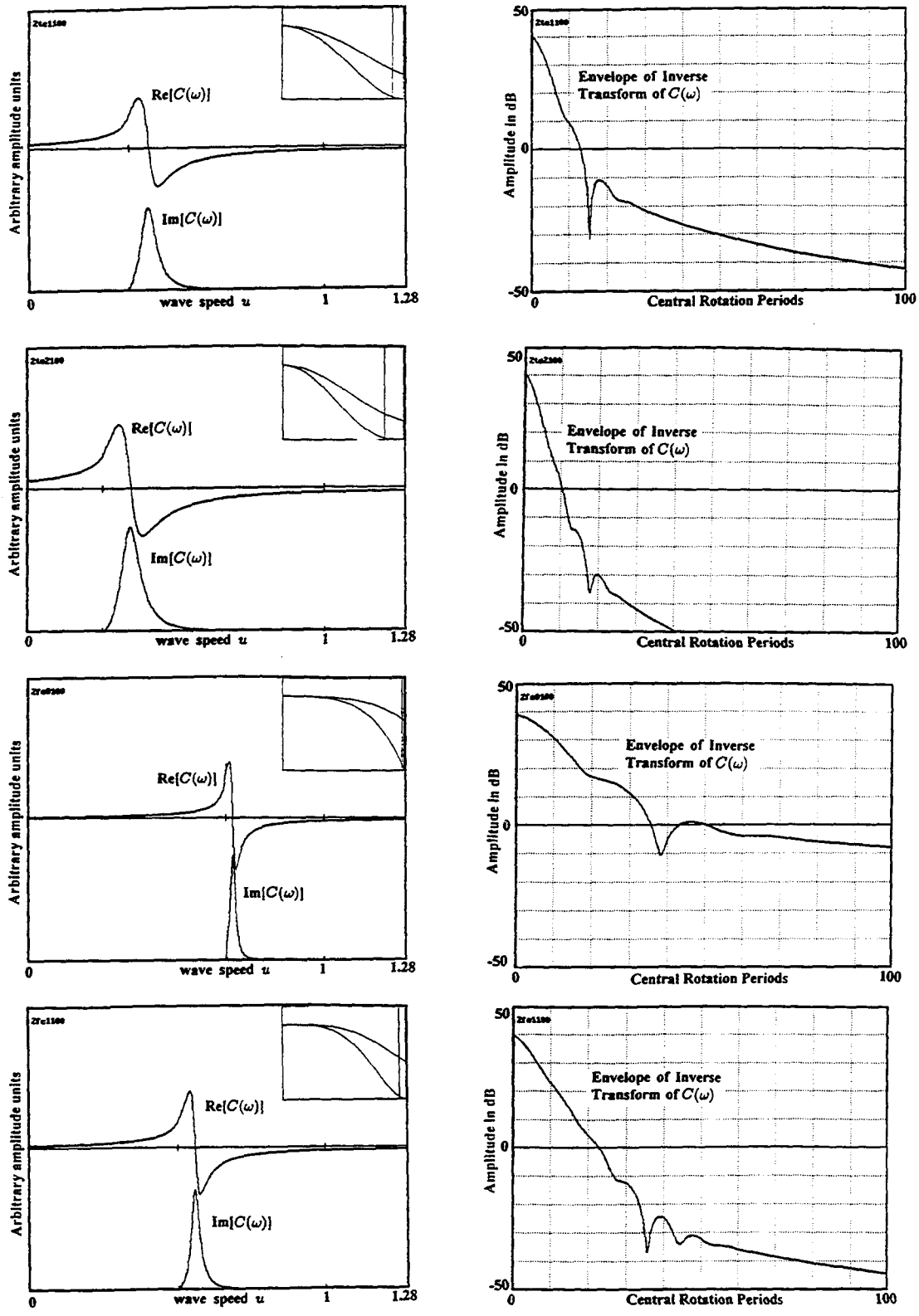

Plate 1. $C(\omega)$ and its inverse Laplace transform for various profiles

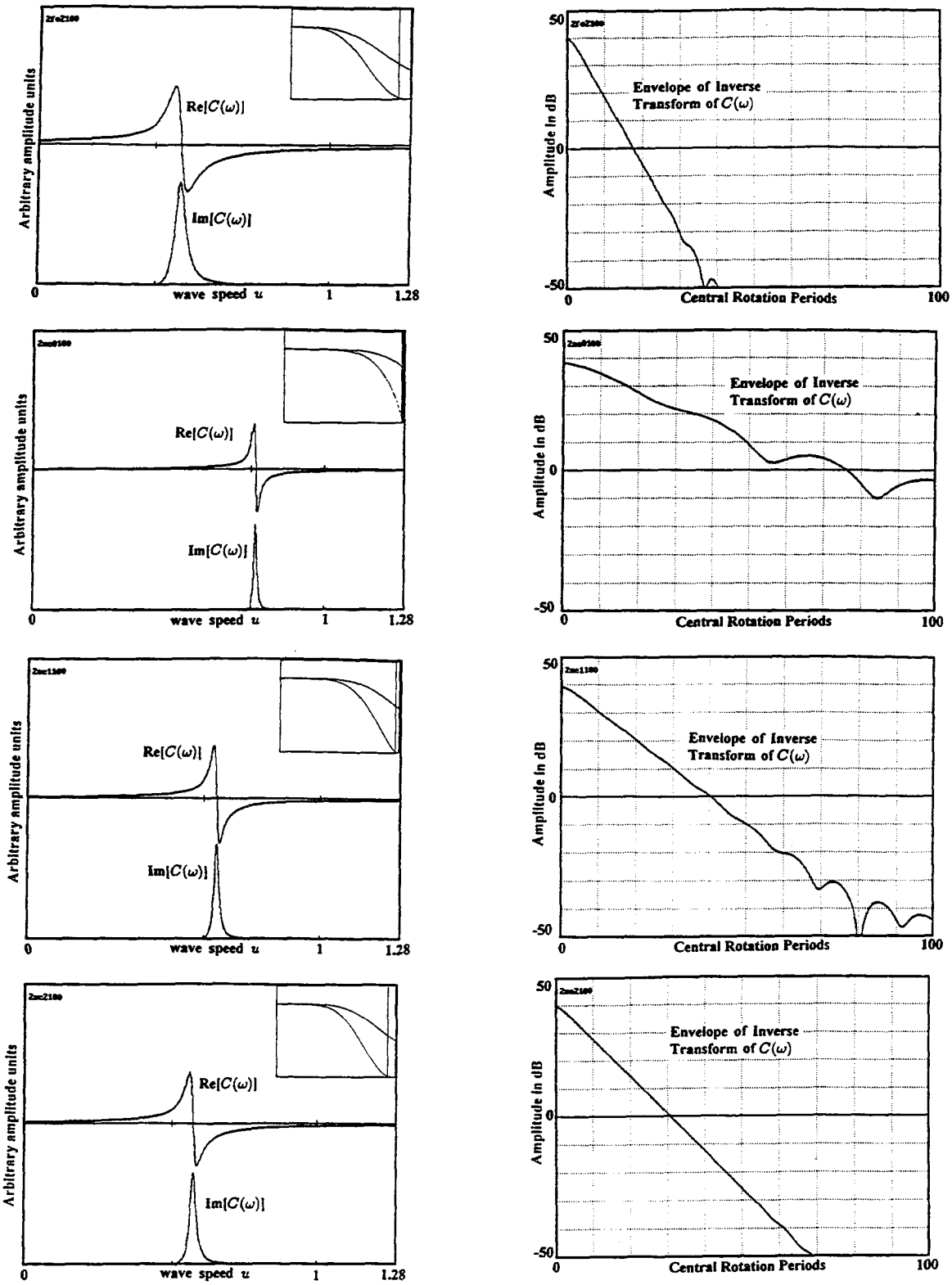

Plate 2. $C(\omega)$ and its inverse Laplace transform for various profiles

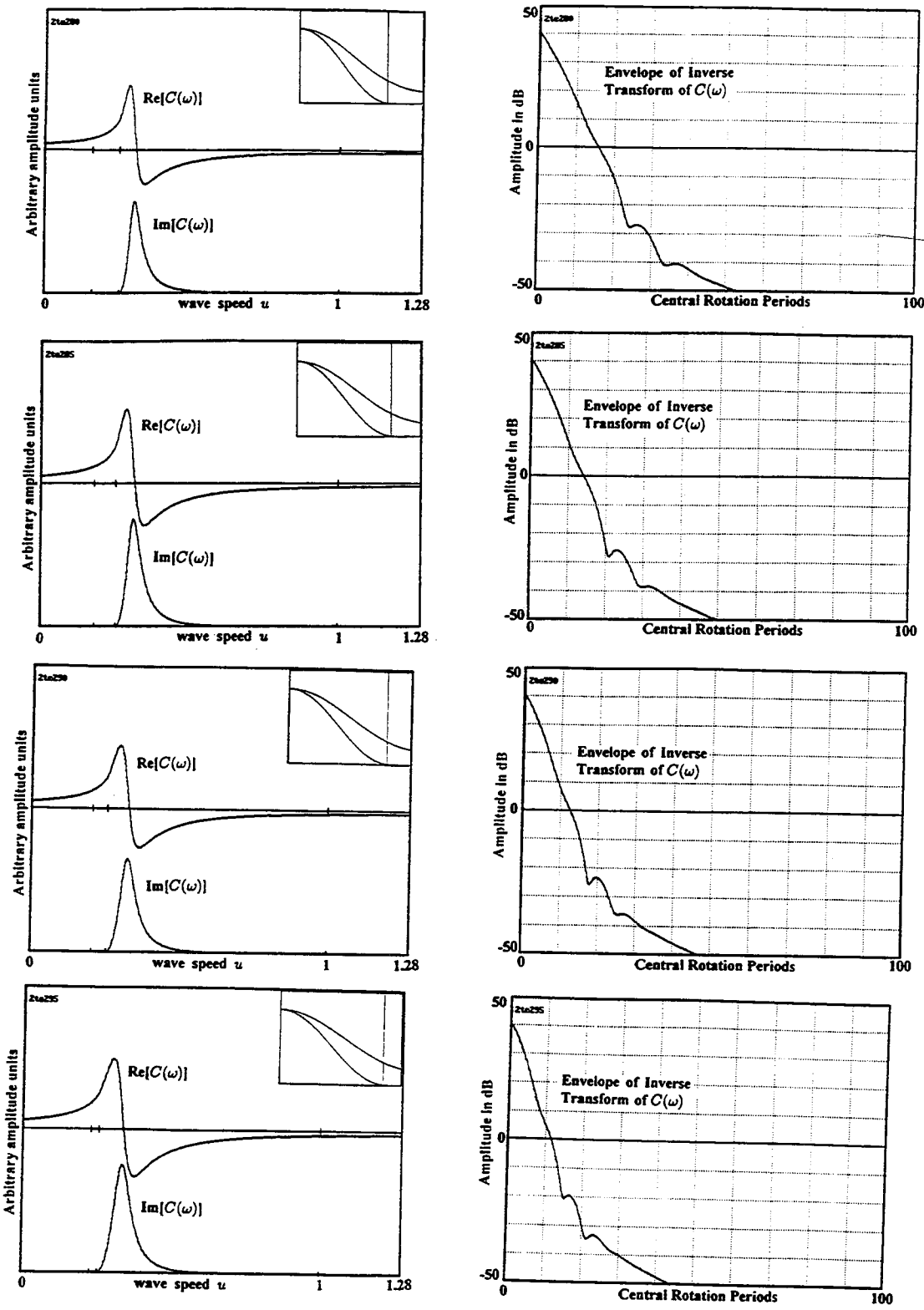

Plate 3. $C(\omega)$ and its inverse Laplace transform for various profiles

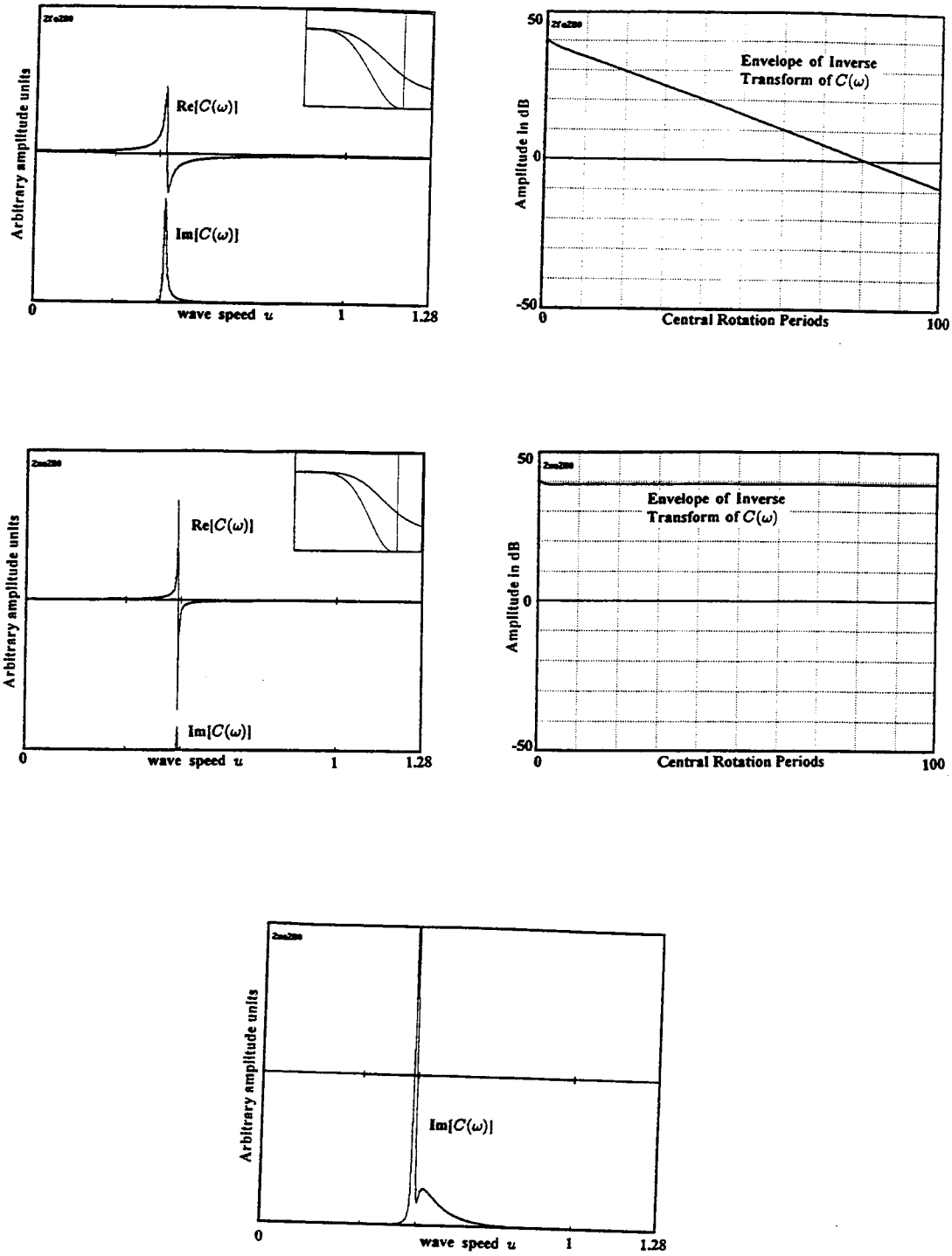

Plate 4. $C(\omega)$ and its inverse Laplace transform for various values of parameter α

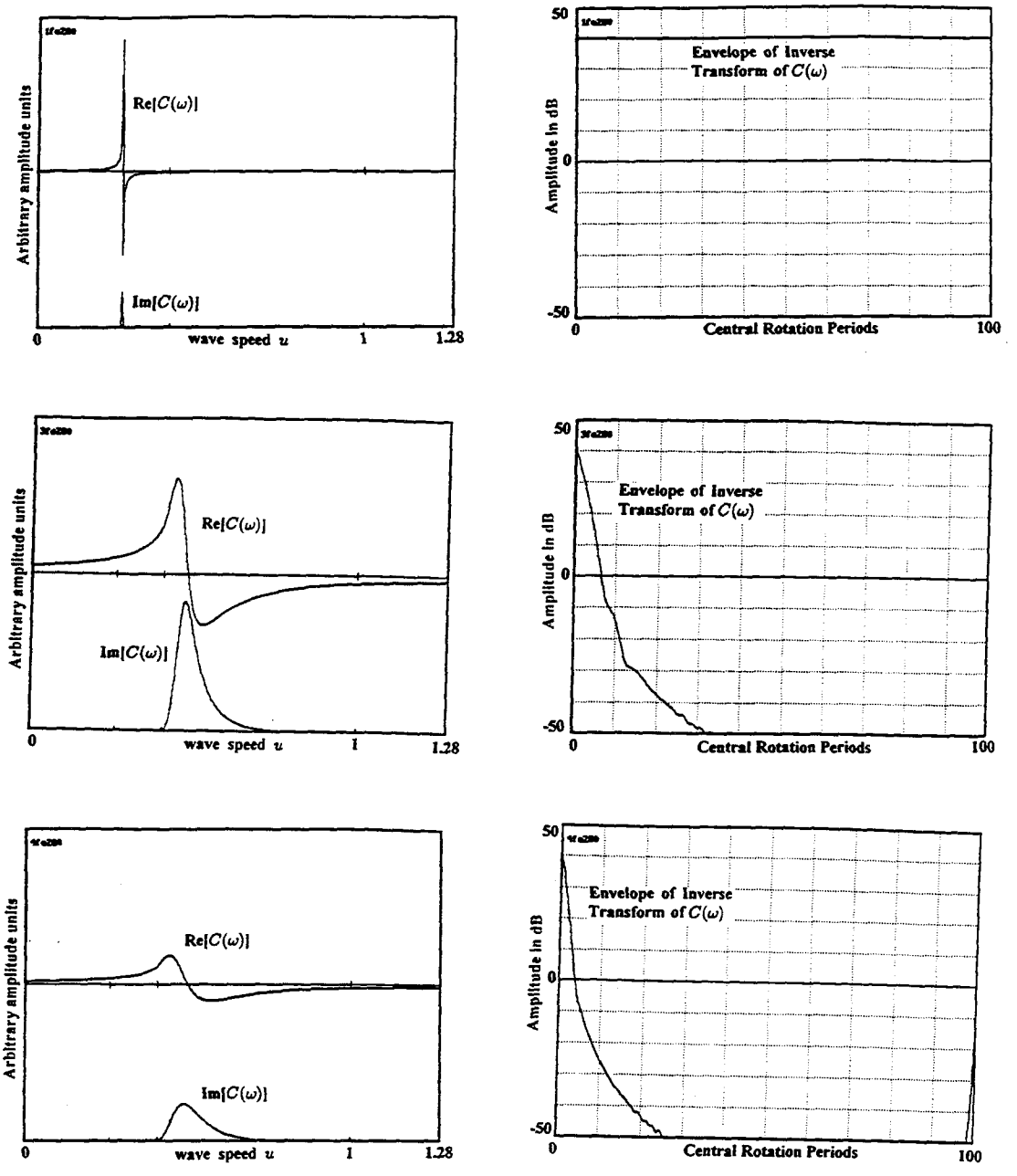

Plate 5. $C(\omega)$ and its inverse Laplace transform for various values of eigen number m

to indicate the central, edge and wall angular velocities. The inset for each drawing of $C(\omega)$ is a plot of the normalized density and velocity profiles used in the calculations. The vertical line in the inset indicates the resonant radius. Plates 1 and 2 show the result for the various tabulated profiles with $\alpha = 1$. Plate 3 shows the effect of α on $C(\omega)$ for the power two (#2) profile. The effect of the azimuthal eigen number m is shown in Plate 5.

5.5 INFERENCES

All the pictures of $C(\omega)$ have the same general shape, which may be approximated by a simple complex pole model like (22). The most significant portion of $C(\omega)$ lies near the plasma edge. When the profile is not smooth, the imaginary part of $C(\omega)$ ends abruptly. The inverse transforms all show an initial fast decay and then an asymptotically slower decay (algebraic). In between the two, there are points where the temporal response suddenly dips. Around this dip, the envelope becomes wavy (perhaps due to some interference between the initial decay and the algebraic decay). The magnitude of the response at which this dip occurs is lower for smoother profiles. The point in *time* at which the dip occurs is larger for flatter profiles (i.e. profiles that are flatter at the origin $\rho = 0$). This means that for profiles that are both smooth and flat, the dip is not noticeable for a wide range of magnitude. The initial fast decay rate is larger for smoother profiles. But the initial decay rate is smaller for flatter profiles. Profiles that are both flat and smooth show responses that have an initial decay that is exponential.

The parameter α does not seem to have such a profound effect on either $C(\omega)$ or its inverse transform. However, it is observable that the profiles with a lower α have a lower initial decay rate. A comparison of the bottom figures on Plates 2 and 4 show that although the $m = 2$ response for a power six (#2) profile with $\alpha = 1$ is damped, for $\alpha = 0.8$ the $m = 2$ response is undamped! A study of $C(\omega)$ for the 2se280 profile on Plate 4 shows that the diocotron resonance occurs at a radius outside the plasma edge.

A special mention must be made about $C(\omega)$ for an undamped response. In calculating $C(\omega)$, it was assumed that Im[u] > 0. Hence the imaginary part of $C(\omega)$ is not a delta function, as would be expected if the inverse Fourier transform of $C(\omega)$ were an undamped sinusoid. Moreover, the discrete nature of the calculation does not do justice to the proper representation of a narrow peaked response. Hence the amplitude of the imaginary part of $C(\omega)$ should be much larger than shown.

The bottom Figure in Plate 4 is $C(\omega)$ for the power six (#2) profile with $\alpha = 0.8$, but plotted on a much larger scale (i.e. increased magnification). Observation shows an additional peak for Im[$C(\omega)$], but this peak has a much broader width. The inference is that for this particular case, two distinct diocotron resonances are possible. The second resonance is a comparatively highly damped and occurs at a larger frequency. Hence the temporal response will be dominated by the undamped resonance.

The Q of the resonance for these different profiles vary widely from $Q = 4.5$ for the $m = 2$ in the power two (#2), $\alpha = 1.0$, case to a $Q = \infty$ for undamped resonances. The $m = 2$ diocotron in a power four (#2) profile with $\alpha = 0.8$ has a $Q = 42$ which matches the experimentally obtained value.

5.6 DISPERSION OF DIOCOTRON WAVES

The effect of exciting different quasimodes, specifically the $m = 1$, $m = 3$ and the $m = 4$, on the power four (#2) profile with $\alpha = 0.8$ is shown in Plate 5. Of the three marks in the central horizontal line of the figure for $C(\omega)$, the leftmost corresponds to $g(1)$ and the middle one is $g(\alpha)$. It is seen that the $m = 1$ resonance occurs at the wall rotation frequency and it is undamped. The $m = 3$ and $m = 4$ resonances occur within the plasma. The damping rate of the $m = 3$ is smaller than that of the $m = 4$. And these two resonances occur more or less around the same radius. However, it must be noted that the $m = 3$ frequency is only about $3/4$ of the $m = 4$ frequency. A detailed study of the

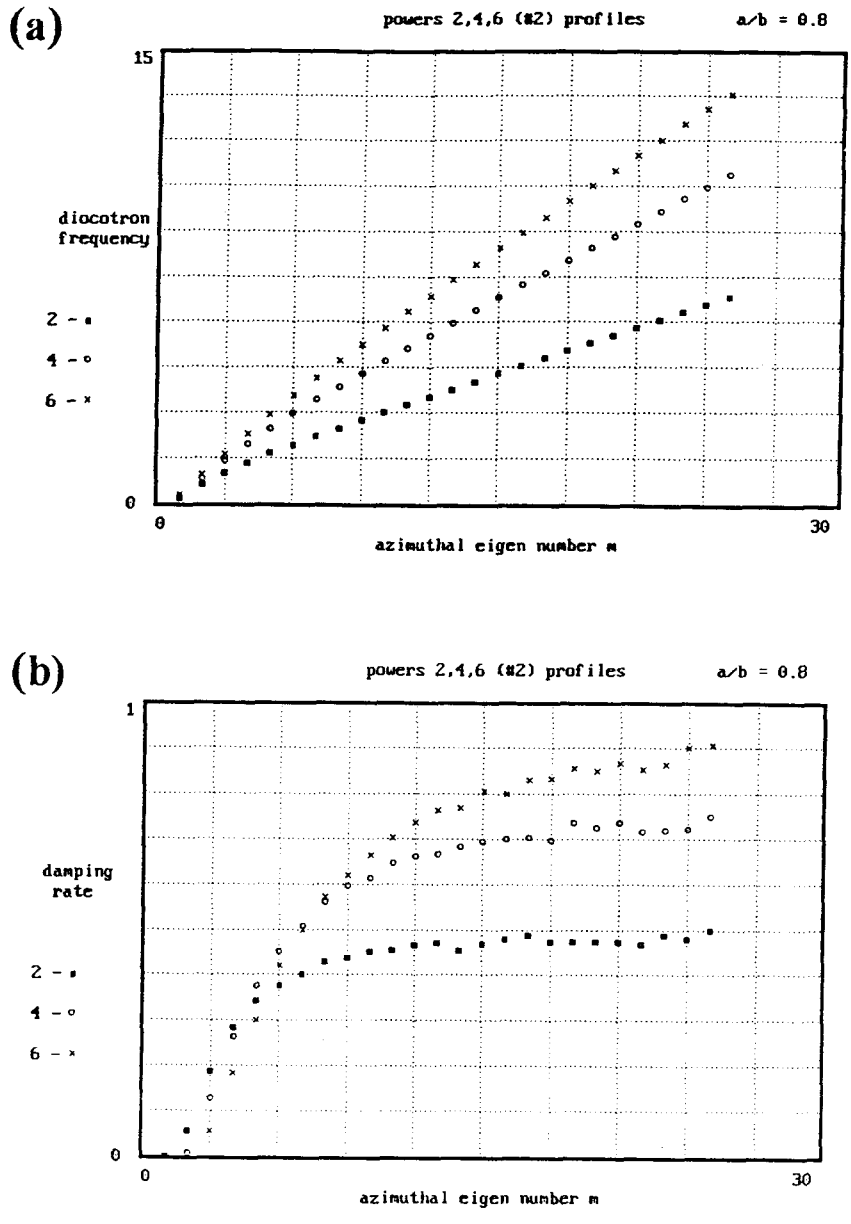

Figure 21. (a) Variation of the diocotron frequency with azimuthal eigen number m for selected profiles with $\alpha = 0.8$. All frequency values are normalized to the central rotation frequency $\omega_0(0)$. (b) Variation of normalized damping rate with m number for the same cases as in (a) above. Together, these graphs give an idea of the dispersion of the diocotron waves by the plasma. The frequency and damping rate are the parameters that describe the initial fast (exponential) decay of the diocotron wave, and are the values that would be inserted into the electrical model of the plasma represented by the simple complex pole model for the capacitance function as shown in equation (22).

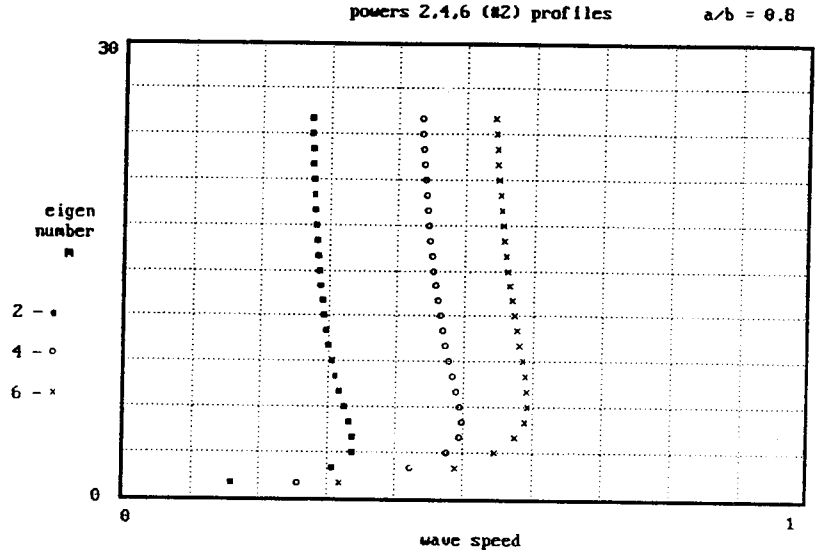

Figure 22. The diocotron frequency, as represented in equation (22), is the angular velocity of the resonant radius where the wave speed equals the angular velocity. The above graph shows the variation of the resonant radius with the mode number.

quasimodes with different azimuthal eigen numbers was carried out with a motivation to find out, qualitatively, the dispersion for diocotron waves in a pure electron plasma. The results are shown in Figures 21(a) and (b). Computations were made on powers 2, 4 and 6 (#2) profiles, all with $\alpha = 0.8$. The behavior of the diocotron wave for different eigen numbers is more or less the same for different profiles, as may be seen from the graph of quasimode frequency versus eigen number and quasimode damping versus eigen number. The quasimode frequency is approximately proportional to the eigen number with larger slopes for flatter profiles. The damping rate is more complicated. It initially increases with eigen number, but remains constant for high numbers.

Figure 22 shows the variation of the diocotron frequency with the wave speed of the diocotron resonances. The initial transient response of the diocotron wave is localized to a resonant radius of the plasma where the wave speed equals the angular rotation frequency. Hence the wave speed is an indication of the radius of the plasma that resonates with the diocotron wave. Figure 22 thus depicts the variation of resonant radius with the eigen number. It shows that for a given profile, the resonant radius first moves inward as the mode number increases up to $m = 4$. For higher eigen numbers, the resonant radius moves outward, but not out to the wall. There is no dramatic change of resonant radius with very high eigen numbers.

One parameter not shown in the figures is the relative amplitude of the response for different eigen numbers in the same profile. This is related to the value of B in equation (22) and to the argument of the sine function in equation (21). The relative amplitude of the transient response decreases with increase in eigen number. As an example, the peak of Im$[C(\omega)]$ for the $m = 2$ quasimode in a 2te280 profile is higher by a factor of 15 than the peak of Im$[C(\omega)]$ for the $m = 4$ quasimode in the same profile. The result is that when a plasma is excited by a delta function, although all the diocotron quasimodes may be excited within the plasma, the transient response observed at the wall will be dominated by the quasimodes with lower eigen numbers.

5.7 ALGEBRAIC DECAY

Almost all the results in Plates 1-5 seem to show that the transient response has a sudden dip in amplitude at some point followed by an asymptotic algebraic decay. Both the rate of the decay as well the point in time where the transition occurs is profile dependent. It was surmised that the dip was caused by an interference between the sinusoid of the exponential decay and that of the algebraic decay. It was decided to measure the frequencies of the algebraic and exponential parts. It was found that for the simple power two, power two (#1) and the power two (#2) (all with $\alpha = 1$), and also the power two (#2) with $\alpha = 0.8$ profiles, the ratio of the frequencies of the fast decay to the algebraic decay was in the ratio of the $m = 2$ diocotron frequency to m times the edge rotation frequency for that profile. Since we know the frequency during the fast decay corresponds to the $m = 2$ diocotron frequency, this means that the frequency of the transient response changes from the $m = 2$ frequency before the dip to m times the edge frequency after the dip. And the dip was caused by destructive interference between the two frequencies. We can now surmise the following:

The transient response of the plasma to a diocotron wave consists of two distinct frequency components in the asymptotic limit:

$$d(t) = D_m e^{-\gamma_m t} \sin\left[\omega_m t\right] + D_a h(1/t) \sin\left[m g(\alpha) t\right]$$

where D_m and D_a are complex constants (providing phase and amplitude information) and $h(1/t)$ is a polynomial in $1/t$ (which is valid only in the asymptotic limit). The first term is caused by the diocotron wave speed resonating with a particular radius of the plasma. The resonant frequency is m times the angular velocity of the resonant radius. The second term may be the result of the diocotron wave interacting with the rest of the plasma. Since the second term is valid only for large t, around $t = 0$ the exponential term dominates and the transient response is simply that of the first term. At some point in time, the algebraic and exponential parts become commensurate in amplitude and interfere

providing the waves around the dip as seen in Plates 1-5. The dip occurs when phasor addition of the two terms cause destructive interference. In the asymptotic regime, the algebraic decay dominates.

Both Case and Briggs *et al.* predicted, on purely mathematical grounds, the presence of the algebraic decay [1, 2]. They ascribed it to the contribution of the *continuum*, or the collective contribution of the entire range of angular velocities of the plasma $m\omega_0(\rho)$ with $0 \leq \rho \leq \alpha$. However, they do not consider any particular density or angular velocity profile and base their arguments on general grounds. They also do not suggest any reason why the algebraic decay should be dominated by m times the edge frequency. Based on the results in Plates 1-5, it is our hypothesis that the algebraic decay should disappear for density profiles that are very flat at the origin and analytic in the region around $\rho = \alpha$.

5.8 NEGATIVE ENERGY EXPLAINED

Chapter 3 contained the details of an experiment that showed that when dissipation is introduced at the wall of the electrode, the decay rate of the $m = 2$ diocotron wave decreased. From this, it was confirmed that the $m = 2$ diocotron wave was a negative energy wave. This had been experimentally verified for the $m = 1$ diocotron, and theoretically predicted for diocotron waves that were undamped [2, 3]. Described below is a model for understanding the negative energy behavior of the quasimode based on the Lorentzian model of the capacitance function developed in this chapter.

Figure 14(a) shows an octupole sector of the electrode structure connected to a resistor R. This represents what was performed experimentally to confirm the negative energy behavior. At the junction between the electrode and the resistor, the following equation is valid:

$$Y(\omega) + \frac{1}{R} = 0.$$

Using equation (22) representing the Lorentzian model of the capacitance function and solving for ω in the above equation, we get:

$$\omega = \frac{1}{1+(KR)^2}[\omega_2 - \gamma_2 KR - i(\gamma_2 + \omega_2 KR)] \tag{23}$$

where $K = ABF^2$ (A and F are defined in (21) and B is defined in (22)). Since A is a positive constant, $K < 0$ because $B < 0$ from fitting the model equation (22) to the actual plot of $C(\omega)$. Experimentally, from Figure 15, KR is determined to have a value around 0.01. Hence the above equation simplifies to

$$\omega \approx \omega_2 - i(\gamma_2 + \omega_2 KR). \tag{24}$$

Equation (23) shows that in the presence of wall dissipation, both the frequency and the damping rate are changed. Since $KR \ll 1$, the shift in the $m = 2$ frequency is not significant. The damping rate is changed significantly when $\omega_2 \gg \gamma_2$ (which is satisfied in the experiments), and it should decrease with increase in resistance. Equation (24) shows that the decrease in damping rate should be linear with increase in resistance. This is not inconsistent with the experimental result seen in Figure 15. This is true for any diocotron quasimode which can be approximated with the model equation (22) with $B < 0$. As seen from the figures in Plate 5, this is true for the higher quasimodes with $m = 3$ and 4. Hence these, and other similar quasimodes, will also be negative energy waves and their damping rate will decrease with the addition of an external resistance.

REFERENCES

[1] K.M. Case, Phys. Fluids **3**, 143 (1960)

[2] R.J. Briggs, J.D. Daugherty, and R.H. Levy, Phys. Fluids **13**, 421 (1970)

[3] W.D. White, J.H. Malmberg, C.F. Driscoll, Phys. Rev. Lett. **49**, 1822 (1982)

CHAPTER 6

CONCLUSION AND FUTURE WORK

6.1 CONCLUSION

A pure electron plasma can be confined by means of static electric and magnetic field within a cylindrical Penning trap. The radius of the confined plasma may not extend all the way up to the wall. When so confined, the plasma will be in steady-state rotation about the axis of the cylinder. The dynamics of such a plasma, under certain approximations, in the two-dimensional (r, θ) plane is mathematically analogous to the dynamics of 2-D inviscid incompressible fluid flow. This analogy allows us to relate the electrostatic potential to the stream function and the density to fluid vorticity. The angular velocity of rotation of the fluid is a function of the density (vorticity) profile.

For monotonically decreasing angular velocity profiles, experiments reveal the existence of resonant frequencies at integral multiples of the angular rotation frequency, and much below the single particle cyclotron frequency. These resonances, the diocotron resonances, may be considered to be excited at a resonant radius where the diocotron frequency is m times the angular velocity at that radius. When the plasma is excited by an azimuthally traveling electric field propagating of azimuthal eigen number m, with a wave speed equal to the angular velocity of the resonant radius, a sinusoidal current will be induced at the wall of the electrode. If the source of excitation is removed, and the walls of the electrode are perfectly conducting, the induced current may or may not decay. Experiments show that the $m = 2$ resonance induces a current that decays with time. In the linear regime of the experiment, the $m = 2$ response decays exponentially. The time taken by an $m = 2$ resonance to decay to $1/e$ of its initial value is much less than the time between collisions of the particles. Hence this decay is *collisionless*. When the excitation amplitude is large enough to cause non-linear behavior, the induced current is no longer an

exponentially decaying sinusoid but is modulated by trapped fluid oscillations around the resonant radius of the plasma.

That the decay of the diocotron wave is not caused by wall dissipation is borne out by another experiment that shows that the addition of wall resistance causes the damping rate of the $m = 2$ diocotron wave to *decrease*. Hence the $m = 2$ diocotron wave is a *negative energy* wave. Experiments also showed that it was possible to destabilize an otherwise damped diocotron resonance. This may be done by providing sufficient wall dissipation.

A self-consistent set of equations for the linear perturbed potential using the fluid model of the non-neutral plasma reveals the diocotron equation, which is quite similar to the Rayleigh equation for a 2-D inviscid, incompressible fluid. The uniqueness of the equation lies in a singularity when the frequency of the perturbation, ω, equals m times the angular velocity, $\omega_0(r)$. Solution of the equation for a particularly simple parabolic profile with the homogeneous boundary conditions and extension of the radius variable, r, to the complex domain reveals a complex eigenvalue for ω. The sign of the imaginary part of ω is such as to cause damping of the perturbation. The ratio of the real part to the imaginary part of ω is within a factor of 3 of the experimental result. Previous theoretical prediction based on the kinetic model of the plasma revealed a damping rate which was two orders of magnitude away from the corresponding experimental result.

Computations carried out with different density profiles show that the resonant frequency and the damping rate are dependent on the smoothness and flatness of the profile. Computations supported the theoretical finding of an eigenvalue and provided a profile with a ratio of resonant frequency to damping rate that matched the experimental result. It also revealed that diocotron resonances can occur outside the plasma edge. Further analysis showed that the transient response should decay initially with an exponential rate, but asymptotically the decay would be algebraic. The frequency of the algebraic decay is m times the angular velocity of the plasma edge. The point of transition

from a fast exponential decay to a slow algebraic one is dependent on the profile. For smoother and flatter profiles, the algebraic decay cannot be seen experimentally.

The diocotron resonance may be understood by representing the plasma admittance function as one with a simple complex pole in the frequency domain. With such a representation, it is confirmed that a decrease of wall conductivity should have the effect of decreasing the damping rate of the mode. The Lorenztian model of the admittance function of the plasma for diocotron resonances show that this behavior is common to all diocotron modes, not just the $m = 1$ and $m = 2$.

6.2 FUTURE WORK

The studies on the diocotron resonance is not by any means over. It was shown that the experimental observations of the diocotron resonances could be explained on the basis of the linear fluid model using the drift approximation. This latter approximation neglects inertial effects like Coriolis and centripetal forces. The drift approximation also neglects collective effects of viscosity and pressure, both thermal in origin. Calculations show that inertial effects in our plasma are larger in magnitude than thermal effects. These thermal effects are responsible for changing higher eigenmodes of the cyclotron resonances to propagating Bernstein modes [1]. It is not known what effects the inertial and thermal effects have on diocotron quasimodes. Ironically, observations of the linear damping do not reveal any phenomena which may suggest revising the model to include higher order effects.

Viscosity is a dissipative mechanism. Since diocotron waves are negative energy waves, one would expect viscosity to decrease the damping rate of the resonances. This must be tested experimentally.

As stated above, an innocuous damped $m = 2$ resonance can be destabilized into a growing mode by the addition of sufficiently high wall resistance. If viscosity does decrease the damping rate of the resonance, then a high enough viscosity should result in

spontaneous diocotron resonances. Although the viscosity in a non-neutral plasma may not be so high, this may find application in the study of viscous fluid instabilities.

It has already been observed that axial motion will cause damping of the $m = 1$ diocotron resonance. No work has been done to see if the quasimodes are also affected in a similar way by including axial motions [2].

REFERENCES

[1] R. W. Gould and M. A. LaPointe, Phys. Fluids B **4**, 2038 (1992)

[2] B. Cluggish, Bull. Am. Phys. Soc. **38**, 1972 (1993)

APPENDIX

Derivation of the admittance function $Y(\omega)$

Referring to figure 18(a) and (b), if $V(\omega)$ is the voltage applied to the octupole and $\phi(m, k, \omega)$ are the Fourier components of the plasma potential at the wall, then:

$$V(\theta, z, \omega) = \sum_k \sum_m \phi(m, k, \omega) e^{im\theta} e^{ikz}$$
$$= \sum_n \sum_m \phi(m, n, \omega) e^{im\theta} e^{i2\pi nz/L}.$$

Then

$$\frac{1}{L}\int_{-\frac{L}{2}}^{+\frac{L}{2}} V e^{-i2\pi nz/L} dz = \sum_m \phi(n, m) e^{im\theta}.$$

Because $V = 0$ for $-\frac{L}{2} < z < -l$ and $0 < z < \frac{L}{2}$, we have

$$\frac{1}{L}\int_{-l}^{0} V e^{-i2\pi nz/L} dz = \frac{V}{L}\int_{-l}^{0} V e^{-i2\pi nz/L} dz$$

$$= \frac{V}{L}\frac{e^{i2\pi nl/L} - 1}{i2\pi n/L}$$

$$= \frac{lV}{L}\frac{\sin(n\pi l/L)}{n\pi l/L} e^{i2\pi nl/2}.$$

We are interested in modes with $n = 0 \Rightarrow \sin(n\pi l/L)/(n\pi l/L) \rightarrow 1$. Hence

$$\frac{1}{L}\int_{-l}^{0} V e^{-i2\pi nz/L} dz = \frac{lV}{L} = \sum_m \phi e^{im\theta}$$

where it is understood that $\phi(m, \omega) = \phi$. Then

$$\phi = \frac{l}{L}\frac{1}{2\pi}\int_{-\frac{\pi}{8}}^{\frac{\pi}{8}} V e^{-im\theta} d\theta$$

$$\Rightarrow \qquad V(\theta,\omega) = \frac{2\pi}{m/2}\,\frac{\phi(m,\omega)}{\frac{l}{L}\sin(m\pi/8)}. \tag{B1}$$

Equation (B1) gives the relation between the voltage applied to the octupole and the plasma potential at the wall of the electrode. Now, to find out the relation between the current $I(\omega)$ and the electric field E_r at the wall. From an application of Ampere's law applied to electrode wall:

$$\nabla \times \vec{H} = \vec{J} + \epsilon_0 \frac{\partial \vec{E}}{\partial t}$$

$$\Rightarrow \qquad \nabla \cdot \left(\vec{J} + \epsilon_0 \frac{\partial \vec{E}}{\partial t}\right) = 0$$

$$\Rightarrow \qquad \int \left(\vec{J} + \epsilon_0 \frac{\partial \vec{E}}{\partial t}\right) \cdot \vec{ds} = 0$$

$$\Rightarrow \qquad \int \vec{J} \cdot \vec{ds_1} + \epsilon_0 \frac{\partial}{\partial t} \int \vec{E} \cdot \vec{ds_2} = 0$$

where the first integral is evaluated over the area of the outer octupole surface area carrying the current I and the second integral is evaluated over the inner octupole surface area facing the plasma.

$$\Rightarrow \qquad -\int J_r ds_1 - \epsilon_0 \frac{\partial}{\partial t} \int E_r ds_2 = 0.$$

The negative sign comes in the first integral because the outward surface element vector located at the outer surface of the octupole (facing the wire) is opposite in direction to the current density in the wire.

$$\Rightarrow \qquad -I - \epsilon_0 \frac{\partial}{\partial t} \int_{-\frac{\pi}{8}}^{\frac{\pi}{8}} E_r e^{im\theta} bl d\theta = 0$$

or $$I = -\epsilon_0 \left(\frac{\partial E_r}{\partial t}\right) \frac{2bl}{m} \sin(m\pi/8)$$

i.e. $$I(\omega) = i\omega\epsilon_0 \frac{2bl}{m} E_r \sin(m\pi/8) \tag{B2}$$

where it is understood that the electric field is to be evaluated at the wall. From equations (B1) and (B2), we get:

$$Y(\omega) \equiv \frac{I(\omega)}{V(\omega)} = \frac{i\omega\epsilon_0 \frac{2}{m} blE_r \sin(m\pi/8)}{\frac{2}{m} 2\pi \frac{\phi}{\frac{l}{L}\sin(m\pi/8)}}$$

$$= i\omega\left(\epsilon_0 \frac{L}{2\pi}\right)\left(\frac{bE_r}{\phi}\bigg|_{r=b}\right)\left(\frac{l}{L}\right)^2 \sin^2\left(\frac{m\pi}{8}\right)$$

$$Y(\omega) = i\omega AC(\omega)F^2 \tag{B3}$$

where A is a constant with the units of capacitance and F is a geometric form factor. If the plasma were excited with an $m = 2$ configuration, but the response were still obtained with a single electrode, then $Y(\omega)$ would only be altered by numerical constants, a factor of 4 in this case. $C(\omega)$ is a dimensionless quantity, which is shown below to be a dimensionless ratio of the electric field to the potential at the wall. It may be considered as a dimensionless capacitance function. $AC(\omega)$ would have the dimensions of capacitance.

$$C(\omega) = \frac{bE_r(r)}{\phi(r)}\bigg|_{r=b} = \frac{-b}{\phi(r)}\frac{d\phi(r)}{dr}\bigg|_{r=b} = \frac{-1}{\phi(\rho)}\frac{d\phi(\rho)}{d\rho}\bigg|_{\rho=1} = \frac{E_\rho(\rho)}{\phi(\rho)}\bigg|_{\rho=1}$$

Equation (B3) gives the admittance function of the pure electron plasma. Of the quantities involved in the calculation of $Y(\omega)$, only $C(\omega)$ is unknown. This may be calculated by the method outlined in Chapter 5.